

1           **Seasonal variations in metallic mercury (Hg<sup>0</sup>) vapor**  
2           **exchange over biannual wheat - corn rotation cropland in**  
3           **the North China Plain**

4  
5           **J. Sommar<sup>1</sup>, W. Zhu<sup>1,\*</sup>, L. Shang<sup>1</sup>, C. -J. Lin<sup>1,2,3</sup> and X. B. Feng<sup>1</sup>**

6  
7           <sup>1</sup>State Key Laboratory of Environmental Geochemistry, Institute of Geochemistry, Chinese Academy  
8           of Sciences, Guiyang 550002, China.

9           <sup>2</sup>Department of Civil and Environmental Engineering, Lamar University, Beaumont, TX 77710,  
10          United States.

11          <sup>3</sup>College of Environment and Energy, South China University of Technology, Guangzhou 510006,  
12          China.

13          \*Now at: Department of Chemistry, Umeå University, 901 87 Umeå, Sweden

14          Correspondence to: J. Sommar ([jonas@mail.gyig.ac.cn](mailto:jonas@mail.gyig.ac.cn)) and X. B. Feng ([fengxinbin@vip.skleg.cn](mailto:fengxinbin@vip.skleg.cn))

## 15 **Abstract**

16 Air-surface gas exchange of  $\text{Hg}^0$  was measured in five approximately bi-weekly campaigns (in total 87  
17 days) over a wheat-corn rotation cropland located in the North China Plain using the relaxed eddy  
18 accumulation (REA) technique. The campaigns were separated over duration of a full year period (2012 -  
19 2013) aiming to capture the flux pattern over essential growing stages of the planting system with a low  
20 homogeneous topsoil Hg content ( $\sim 45 \text{ ng g}^{-1}$ ). Contrasting pollution regimes influenced air masses at the  
21 site and corresponding  $\text{Hg}^0$  concentration means (3.3 in late summer to  $6.2 \text{ ng m}^{-3}$  in winter) were  
22 unanimously above the typical hemispheric background of 1.5 -  $1.7 \text{ ng m}^{-3}$  during the campaigns.  
23 Extreme values in bi-directional net  $\text{Hg}^0$  exchange were primarily observed during episodes of peaking  
24  $\text{Hg}^0$  concentrations. In tandem with under-canopy chamber measurements, the above-canopy REA  
25 measurements provided evidence for a balance between  $\text{Hg}^0$  ground emissions and uptake of  $\text{Hg}^0$  by the  
26 developed canopies. During the wheat growing season covering  $\sim 2/3$  of the year at the site, net field-scale  
27  $\text{Hg}^0$  emission was prevailing for periods of active plant growth until canopy senescence (mean flux:  $20.0$   
28  $\text{ng m}^{-3}$ ) disclosing the dominance of  $\text{Hg}^0$  soil efflux during warmer seasons. In the final vegetative stage of  
29 corn and wheat, ground and above-canopy  $\text{Hg}^0$  flux displayed inversed daytime courses with a near mid-  
30 day maximum (emission) and minimum (deposition) respectively. In contrast to wheat,  $\text{Hg}^0$  uptake of the  
31 corn canopy at this stage offset ground  $\text{Hg}^0$  emissions with additional removal of  $\text{Hg}^0$  from the  
32 atmosphere. Differential uptake of  $\text{Hg}^0$  between wheat ( $\text{C}_3$  species) and corn ( $\text{C}_4$  species) foliage is  
33 discernible from estimated  $\text{Hg}^0$  flux (per leaf area) and Hg content in mature cereal leaves being a factor  
34 of  $> 3$  higher for wheat (at  $\sim 120 \text{ ng g}^{-1}$  dry weight). Furthermore, this study shows that intermittent flood  
35 irrigation of the air-dry field induced a short pulse of  $\text{Hg}^0$  emission due to displacement of  $\text{Hg}^0$  present in  
36 the surface soil horizon. A more lingering effect of flood irrigation is however suppressed  $\text{Hg}^0$  soil  
37 emissions, which for wet soil ( $\sim 30 \text{ \%}$ -vol) beneath the corn canopy was on an average a factor of  $\sim 3$   
38 lower than that for drier soil ( $< 10 \text{ \%}$ -vol) within wheat stands. Extrapolation of the campaign  $\text{Hg}^0$  flux  
39 data (mean:  $7.1 \text{ ng m}^{-2} \text{ h}^{-1}$ ) to the whole year suggests the wheat-corn rotation cropland a net source of  
40 atmospheric  $\text{Hg}^0$ . The observed magnitude of annual wet deposition flux ( $\sim 8.8 \mu\text{g Hg m}^{-2}$ ) accounted for  
41 a minor fraction of soil  $\text{Hg}^0$  evasion flux prevailing over the majority of year. Therefore, we suggest that  
42 dry deposition of other forms of airborne Hg constitutes the dominant pathway of Hg input to this local  
43 ecosystem and that these deposited forms would be gradually transformed and re-emitted as  $\text{Hg}^0$  rather  
44 than being sequestered here. In addition, after crop harvesting, the practice of burning agricultural residue

45 with considerable Hg content rather than straw return management yields seasonally substantial  
46 atmospheric Hg<sup>0</sup> emissions from croplands in the NCP region.

## 47 **1. Introduction**

48 Mercury (Hg) is an important environmental contaminant because of its cyclic transport between air,  
49 water, soil and biosphere and its tendency to bioaccumulate in the environment as neurotoxic mono-  
50 methylated (CH<sub>3</sub>Hg-) compounds (Driscoll et al., 2013). While assessments of Hg burden in  
51 environmental compartments are rather concordant, the fluxes between them are less well constrained  
52 (Selin, 2009) which specifically concern land ecosystem-atmosphere exchange of Hg<sup>0</sup> (Zhang et al.,  
53 2012). Hg in the biosphere is derived primarily from atmospheric deposition (Grigal, 2003), where  
54 foliar uptake of Hg<sup>0</sup> has been recognized as a principal pathway for atmospheric Hg to enter terrestrial  
55 ecosystems (Frescholtz et al., 2003; Niu et al., 2011; Obrist, 2007). In turn, the availability of soil  
56 (inorganic) mercury to aerial parts of terrestrial plants is generally low and the uptake is mainly  
57 retained in the root zone (Cavallini et al., 1999; Meng et al., 2010; Cui et al., 2014). Accumulated Hg in  
58 foliage is transferred to soil reservoirs via plant detritus (St Louis et al., 2001) or may partially be  
59 released back to the atmosphere (Bash and Miller, 2009). In addition, Hg may enter the foliage by  
60 recycling processes releasing Hg<sup>0</sup> from underlying soil surfaces (Millhollen et al., 2006). In review  
61 (Sommar et al., 2013a), a majority of reported Hg<sup>0</sup> flux measurements over terrestrial soils indicate net  
62 emission in warmer seasons and near-zero fluxes at cold temperatures. Soil-air Hg<sup>0</sup> exchange is  
63 controlled by numerous factors including physico-chemical properties of and abiotic/ biotic  
64 processes in the soil, meteorological conditions and atmospheric composition (Bahlmann et al., 2006;  
65 Carpi and Lindberg, 1997; Engle et al., 2005; Fritsche et al., 2008a; Gustin, 2011; Rinklebe et al.,  
66 2010; Mauclair et al., 2008; Zhang et al., 2008). For bare low Hg-containing soils, Briggs and Gustin  
67 (2013) proposed a conceptual model in that the soil moisture regimes largely dictates the level of Hg<sup>0</sup>  
68 flux. The presence of vegetation has effect on the Hg<sup>0</sup> efflux from ground surfaces by modifying soil  
69 moisture by evapotranspiration as well as reducing light penetration, soil temperature and air mixing.  
70 At landscape scale, Hg<sup>0</sup> net exchange measurements may be made directly, using micrometeorological  
71 (MM) methods above vegetation canopies (Bash and Miller, 2009; Baya and Van Heyst, 2010; Cobos  
72 et al., 2002; Converse et al., 2010; Edwards et al., 2005; Fritsche et al., 2008b; Kim et al., 1995; Marsik  
73 et al., 2005; Sommar et al., 2013b). As for numerous trace gases (Fowler et al., 2009), the exchange  
74 fluxes of Hg<sup>0</sup> vary in sign and magnitude (bi-directional exchange). From MM-flux measurements  
75 covering larger temporal scales, it is inferred that vegetated ecosystems can represent both a source and

76 a sink for Hg<sup>0</sup> over shorter or longer periods, depending on the atmospheric concentration,  
77 meteorology, substrates, climate conditions and plant community composition (Bash and Miller, 2009;  
78 Converse et al., 2010; Lee et al., 2000). However, related Hg<sup>0</sup> flux measurements over managed  
79 ecosystems, such as croplands, are sparse and only at best seasonally resolved (Baya and Van Heyst,  
80 2010). Broader seasonal flux data sets are desirable, since the annual net Hg<sup>0</sup> flux over an ecosystem  
81 may represent a subtle balance between opposing processes (Lee et al., 2000). The assessment of local  
82 Hg balances in agricultural regions is challenging, since during a year, very different and contrasted  
83 conditions are observed from fallow period to the maximum development of crop. The foliar uptake of  
84 Hg<sup>0</sup> by major staple grain crops has been studied at low-moderate (Niu et al., 2011) and at high  
85 exposure treatments of Hg<sup>0</sup> vapor (Browne and Fang, 1978; Du and Fang, 1982). The early work  
86 conducted on cereals in tillering stage suggested that assimilation of Hg<sup>0</sup> increased with Hg<sup>0</sup>  
87 concentration, temperature and irradiation, and is controlled by interior (mesophyll) resistances at  
88 optimal growing conditions. The study of Niu et al. (2011) focusing on wheat and corn indicated a  
89 significant correlation between foliage Hg content and the exposure level of airborne Hg<sup>0</sup> for their  
90 principal growing stages. In a further study, Niu et al. (2014) showed that only a moderate level of Hg<sup>0</sup>  
91 pollution in air (~20 ng m<sup>-3</sup>) was required to induce measureable physiological stress on corn tissue.  
92 China is the largest emitter of atmospheric Hg worldwide due to a rapid expansion in fossil fuel  
93 combustion (one quarter of global coal combustion) and increased industrialization in contrast to  
94 significant reduction in anthropogenic emissions in Europe and North America (Streets et al., 2005). In  
95 addition, China is the world's leading producer and consumer of Hg (U.S.G.S., 2015). Using a broad  
96 set of [Hg<sup>0</sup>]/[CO]-ratio observations, Fu et al. (2015) recently estimated the annual anthropogenic Hg<sup>0</sup>  
97 emission in mainland China at approximately 1140 tons, which is significantly higher than previously  
98 predicted by published emission inventories using activity data (Wang et al., 2014d). This  
99 inconsistency also inferred by Song et al. (2015) may propagate into biased-low source strength  
100 estimates or missing source categories in inventories. Since the elevated Hg deposition deriving from  
101 anthropogenic sources tends to concentrate in labile pools, the potential for high re-emission of Hg<sup>0</sup>  
102 from impacted terrestrial ecosystems in China is substantial (Fu et al., 2012; Smith-Downey et al.,  
103 2010). Investigations by dynamic flux chamber (DFC) technique have revealed comparatively high  
104 Hg<sup>0</sup> efflux from agricultural soils compared to soils in other types of land use in China (Fu et al., 2012;  
105 Fu et al., 2008; Wang et al., 2006; Zhu et al., 2011; Zhu et al., 2015a). Therefore, it may be  
106 hypothesized for related croplands that Hg<sup>0</sup> emissions from soil surface, though plausibly (in part)  
107 recaptured by uptake of the overlying canopy, at times have a major contribution to the net Hg<sup>0</sup>

108 exchange, especially in scant or senescent canopies. Micrometeorological measurements yielding the  
109 net flux from the canopy surface, including both soil and plant exchanges, is thus required to address  
110 the importance of cropland and other agro-ecosystems as sources/sinks of  $\text{Hg}^0$ . In an effort to  
111 investigate  $\text{Hg}^0$  uptake or emission from crop vegetation and soil, we have conducted broad seasonal  
112 measurements of field-scale  $\text{Hg}^0$  flux at three sites in distinctively different agricultural regions of  
113 China with varying level of Hg content in agricultural soil. All the selected sites were located in a rural  
114 environment without discernible adjacent anthropogenic Hg point sources. The well-characterized and  
115 typical rotation croplands investigated include either paddy or dry land cultivation only or a combination  
116 whereof over a year. We focus on the four cash crops (rice, wheat, corn, and oilseed rape) accounting  
117 for the bulk of the planting area in Mainland China. In order to determine the origin of fluxes, we  
118 combined large-scale above-canopy MM-method flux techniques with small-scale automated DFC  
119 measurement at the canopy-floor in the field experiments. In this paper, we report on  $\text{Hg}^0$  flux  
120 measurements in and above a farm field growing winter wheat – summer corn in rotation during five  
121 campaigns (overall 87 sampling days) over the period May, 2012 to April, 2013. The site is located in  
122 central North China Plain (NCP, between 32 – 40°N and 114 – 121°E), which is considered as China's  
123 granary (covering about 180 000 km<sup>2</sup> of farm lands) with about half and a third of the national wheat  
124 and corn production respectively (NBSC, 1998). Besides being a major agricultural base, the NCP  
125 region is heavily populated and industrialized and suffers from serious particulate and photochemical  
126 air pollution (Wang et al., 2014c; Wen et al., 2015). Forthcoming communications will deal with  
127 characteristics of  $\text{Hg}^0$  fluxes measured over subtropical croplands growing either oilseed rape - rice in  
128 rotation or rice as a single crop. Jointly, in these papers, we are presenting growing and non-growing  
129 season  $\text{Hg}^0$  flux patterns and diurnal features. In addition, we address the role of crop vegetation as a  
130 source/sink of  $\text{Hg}^0$  based on an analysis of the measured difference between above-canopy and ground  
131  $\text{Hg}^0$  fluxes. We also attempt to address the impact of field management activities (e.g. harvest, tillering  
132 and irrigation) and abrupt changes in environmental conditions (e.g. intensive precipitation) on  $\text{Hg}^0$  gas  
133 exchange.

## 134 **2. Materials and methods**

### 135 **2.1 Site description**

136 The experimental site Yucheng Comprehensive Experimental Station (YCES, 36°57'N, 116°36'E,  
137 managed by the Chinese Academy of Sciences) is located in an alluvial plain in the lower reaches of  
138 Yellow River, Shandong province, China. There is a typical crop rotation of winter wheat and summer

139 corn in the region without fallow between the crops. The annual mean air temperature and precipitation  
140 depth was  $12.9 \pm 0.8$  °C and  $528 \pm 197$  mm respectively for 2003 - 2012 (Bao et al., 2014). Due to the  
141 East Asia monsoon, the precipitation pattern is largely asymmetric with 60 - 70% of the total concentrated  
142 to July - August. The wheat-growing season (mean length:  $237 \pm 8$  days) is characterized as dry, windy  
143 and with less precipitation ( $108 \pm 238$  mm) whereas the corn-growing season (mean length:  $107 \pm 7$   
144 days) is generally categorized as semi-humid and warm temperate. The upper texture of farmland soil  
145 is a silty loam with a volumetric soil water content at field capacity of  $0.44 \text{ m}^3 \text{ m}^{-3}$  (Li et al., 2010). In  
146 the tillage layer, soil organic content is 1.21% and pH value is about 7.9 (Tong et al., 2014). Especially  
147 for winter wheat, precipitation does not meet crop water demand, so the cropland is flood irrigated  
148 using groundwater during the pre-frost, jointing, and shooting stages of wheat and prior to planting  
149 corn (typically  $\sim 100$  mm per turn). For the period of this field study (May, 2012 to April, 2013, Fig. 1),  
150 harvest and sowing date of wheat was on June, 24 and Oct., 11 respectively. In turn, corn was planted  
151 on June, 28 with a density at  $65000 \text{ plants ha}^{-1}$  and harvested on Oct., 5. Row spacing was  $\sim 25$  cm and  
152 direction was north-south. The total Hg (THg) content in surface soils was uniform across the  
153 measurement fetch (mean:  $45 \pm 3 \text{ ng g}^{-1}$ ,  $n = 29$ , Sommar et al., 2013b).

## 154 **2. 2 Micrometeorological flux measurements and calculations**

155 The site was in the center of a flat  $\sim 15$  ha grain field and a minimum fetch length of at least 130 m in all  
156 directions (Sommar et al., 2013b). From a 6.5 m high flux tower erected permanently over a year-long  
157 period, MM flux measurements were conducted. Sensible heat ( $H^{EC}$ ), latent heat ( $\lambda E^{EC}$ ) and  $\text{CO}_2$   
158 fluxes ( $F_{\text{CO}_2}^{EC}$ ) were measured by the eddy covariance (EC) method using the instrumentation and  
159 protocol described in Sommar et al. (2013b) and Zhu et al. (2015a, b). In order to diminish frequency  
160 response errors, the EC sensor height was adjusted over time (2.1 - 4.2 m) to keep a relative height  
161 between sensors and the canopy of at least  $\sim 1.5$  m during a campaign (Burba, 2013). The frequency  
162 response of the sensor placement over canopy was investigated by spectral analysis of selected 10-Hz  
163 turbulence time series. Analogous to reported in Sommar et al. (2013b), there was over time little  
164 contribution from small eddies occurring above 5 Hz and instrumentation produced in general co-spectra  
165 similar to the references (Kaimal et al., 1972).

166 Up to now, fast high precision detectors for direct background  $\text{Hg}^0$  flux measurements by the preferred  
167 EC method are not available. A principal alternative flux measurement approach is the relaxed eddy  
168 accumulation (REA) technique (Businger and Oncley, 1990). As in EC, REA measurements is performed  
169 at a single point above the surface, but the detector required in EC is substituted by fast response sampling

170 valves. The inlet of an Hg<sup>0</sup>-REA-system was installed at the same height as the EC sensors, with a  
 171 horizontal displacement distance to the EC sensors of 20 cm. The design and operation of the whole-air  
 172 Hg<sup>0</sup>-REA system used in this study has been described in detail by Sommar et al. (2013b). The REA-  
 173 system was specifically adapted to an automatic Hg<sup>0</sup> vapor analyzer (Model 2537B, Tekran Instruments  
 174 Inc.) to measure fluxes and concentrations of Hg<sup>0</sup>. In this system, upward and downward moving air  
 175 created from eddies in the air column are sampled and separated into reservoirs by the sampling valves.  
 176 Updraft and downdraft sampling conditions are dictated by  $w > \bar{w} + 0.3\bar{\sigma}_w$  and  $w < \bar{w} - 0.3\bar{\sigma}_w$   
 177 respectively, where  $\bar{w}$  is the 5-minute running average of  $w$  and  $\bar{\sigma}_w$  is standard deviation of  $w$  over the  
 178 same interval. Hg<sup>0</sup> flux ( $F^{REA}$ ) is determined over 20-min sampling intervals following:

$$179 \quad F^{REA} = \beta_{T_s} \cdot \sigma_w \cdot \underbrace{(\overline{C^\uparrow} - \overline{C^\downarrow})}_{\Delta C_{REA}} \quad (1)$$

180 where  $\sigma_w$  (m s<sup>-1</sup>) is the standard deviation of  $w$ ,  $\overline{C^\uparrow}$  and  $\overline{C^\downarrow}$  are the average mass concentration of Hg<sup>0</sup>  
 181 (at standard temperature and pressure) from updraft and downdraft samples corrected for dilution by zero  
 182 air injection, respectively (ng m<sup>-3</sup>). In turn, the empirical dimensionless parameter  $\beta_{T_s}$  was calculated on-  
 183 line for each averaging period (20 min) according to:

$$184 \quad \beta_{T_s} = \overline{w' T_s'} / \left[ \sigma_w \cdot (\overline{T_s^\uparrow} - \overline{T_s^\downarrow}) \right] \quad (2)$$

185 where  $T_s$  is temperature measured by the sonic anemometer of the EC system (K),  $\overline{w' T_s'}$  is the  
 186 kinematic buoyancy flux derived from EC (K m s<sup>-1</sup>) and  $\overline{T_s^\uparrow} - \overline{T_s^\downarrow}$  ( $\Delta T_{s,REA}$ ) is the average  $T_s$   
 187 difference in between up- and downdraft samples (K). If the on-line calculated  $\beta_{T_s}$  deviated outside a  
 188  $\pm 0.2$  interval of the median, the overall median value (0.46) was implemented in Eq. (1).

189 Bulk canopy conductance for water vapor,  $g_c$  (m s<sup>-1</sup>), was estimated using a rearranged form of the  
 190 Penman–Monteith equation (Dengel and Grace, 2010):

$$191 \quad g_c = \left\{ \left[ \left( \frac{\Delta}{\gamma} \right) \cdot \left( \frac{H^{EC}}{\lambda E^{EC}} \right) - 1 \right] \cdot (1/g_a) + \left( \frac{\rho_a \cdot c_p}{\gamma} \right) \cdot \left( \frac{D_a}{\lambda E^{EC}} \right) \right\}^{-1} \quad (3)$$

192 where  $\Delta$  is the rate of the increase of saturation vapor pressure with air temperature (kPa K<sup>-1</sup>),  $\gamma$  the  
 193 psychrometric constant (kPa K<sup>-1</sup>),  $g_a$  is the aerodynamic conductance (m s<sup>-1</sup>),  $\rho_a$  the density of dry air

194 (mol m<sup>-3</sup>),  $c_p$  the specific heat of air (J mol<sup>-1</sup> K<sup>-1</sup>),  $D_a$  the water vapor saturation deficit (kPa).

195 Aerodynamic conductance was estimated following Thom (1975):

196 
$$g_a = \kappa^2 \cdot u / \left[ \ln \left( (z - d) / z_0 \right) \right]^2 \quad (4)$$

197 where  $\kappa$  is the von Kármán constant (0.41), and  $u$  is the wind speed measured at height  $z$  (m s<sup>-1</sup>).  $z_0$  is the  
198 surface roughness ( $= 0.15 \cdot h_c$ , where  $h_c$  is the mean canopy height) and  $d$  the zero plane displacement  
199 ( $= 0.67 \cdot h_c$ ). In dry, daytime conditions most of the water vapor flux  $E^{EC}$  would derive from stomata,  
200 with only minor contributions from soil and leaf surface evaporation. Consequently, we only choose  
201 daytime conditions (global radiation > 100 W m<sup>-2</sup>) without the presence of a wet canopy to calculate  $g_c$   
202 as a proxy for canopy stomatal conductance. Most of the data were collected under favorable weather  
203 conditions without rainfall and with sufficient global radiation. However, as only a limited set of  $g_c$  data  
204 was obtained from the winter campaign due to wetness constraints and instrumentation malfunction, these  
205 data were not included in any further evaluation (cf. Table 1).

## 206 **2. 3 Ancillary measurements**

207 The REA-EC instrumentation was accompanied by an automatic weather station (HOBO U30-NRC,  
208 Onset Computer Corp., USA) equipped with sensors for bulk air (temperature and humidity), surface  
209 soil (temperature, volumetric moisture content) parameters and leaf wetness as well as sensors for  
210 global radiation (300 - 1100 nm) and photo-synthetically active radiation (PAR, 400 - 700 nm), respectively.  
211 The weather station stored data as 20 min averages with the same time interval as the flux measurements.  
212 Crop leaf area index (LAI) was measured using an area meter (LI-3100, LI-COR Biosciences) weekly  
213 during the growing season.  $h_c$  was recorded at the same time interval. For the measurement campaigns  
214 with developed canopies (1 - 3; See Table 1), concurrent measurements of both above-canopy Hg<sup>0</sup> net  
215 exchange by the REA-system as well as canopy-floor air-soil exchange by a dynamic flux chamber  
216 (DFC, Lin et al. 2012) were conducted with 20-min time resolution. The set-up and operation of the  
217 automatic DFC system has been described elsewhere (Zhu et al., 2015a). Measurement results of air-  
218 soil Hg<sup>0</sup> flux are briefly provided here in connection with the discussion of MM-derived Hg<sup>0</sup> fluxes.  
219 Corn and wheat foliage samples were collected at harvest stage and analyzed for THg content. Event  
220 based Hg wet deposition and precipitation amounts were measured at an adjacent site ~400 m N of the  
221 field site investigated. Methodological details concerning collection and Hg analysis of foliage and  
222 precipitation samples have been described elsewhere (Zhou et al., 2013).



## 223 **2. 4 Post-processing, correction methods and quality assessment of flux data**

224 10 Hz EC flux raw data were post-processed and quality-controlled using the open-source EddyPro 5.0  
225 flux analysis software package (LI-COR Biosciences Inc.). A series of standard data corrections were  
226 implemented described in (Zhu et al., 2015a). Tests were applied on every 20 min fast time series raw  
227 data to qualitatively assess turbulence for the assumptions required (steady-state conditions and the  
228 fulfillment of similarity conditions) for applying MM (e.g. EC and REA methods). Following the basic  
229 system of Mauder and Foken (2004) the resulting flux was marked with a quality flag (either 0, 1 or 2  
230 denoting high, moderate and low quality, respectively).

231 The REA-system enabled a mode (reference sampling) during which air is sampled synchronously  
232 with both conditional inlets (with the dynamic deadband as a threshold). Regularly during the field  
233 campaigns (every 72 h), the REA system was operated in reference sampling mode to correct for minor  
234 bias between the conditional channels in Eq. (1) following Sommar et al. (2013b).

235 In turn, the relative uncertainty in the REA flux ( $\sigma_{F^{REA}}/F^{REA}$ ) was quantified following Kramm et al.  
236 (1999):

$$237 \quad \sigma_{F^{REA}}/F^{REA} = \pm \sqrt{\left(\sigma_{H^{EC}}/H^{EC}\right)^2 + \left(\sigma_{\Delta C_{REA}}/\Delta C_{REA}\right)^2 + 2 \cdot \left(\sigma_{\Delta T_{s,REA}}/\Delta T_{s,REA}\right)^2} \quad (5)$$

238 The procedures we deployed to assess uncertainty in the individual terms are described in Zhu et al.  
239 (2015b). As the sampled air was not dried, derived  $F^{REA}$  was corrected for variations in the water  
240 vapor content of the air following Lee (2000).

## 241 **3. Results**

### 242 **3. 1 Flux data coverage, detection limit and uncertainty level**

243 Five separate flux measurement campaigns were conducted over the period May 2012 to April 2013.  
244 The time and duration of the campaigns is listed in Table 1, which also include the flux data coverage  
245 for the individual sampling periods. The total flux data coverage across the five campaigns was ~73%.  
246 Gaps in the measurements mainly resulted from power failures, calibration/reference sampling periods  
247 and instrumentation failures. Precipitation events leading to malfunction of the sonic anemometer  
248 contributed to ~15% of the missing data. Extreme imbalances in REA up- and down-draft sampling  
249 volumes on undiluted basis could prevail periodically during very calm wind conditions. This translates  
250 into sub-optimal Hg mass loadings for analysis per sample concerning the channel associated with  
251 small volumes, which potentially yield a biased determination of  $\Delta C_{REA}$  (Zhu et al., 2015b). Data

252 from 20 min periods were not further processed when one of the REA channels was open for sampling  
 253 less than 10% of total time, which accounted for ~12% of missing data. Based on the quality flag of  
 254  $H^{EC}$  data, the percentage of flux data linked with moderate to high quality turbulence during a  
 255 campaign is given in Table 1. Overall, ~70% of flux data belongs to this category.

256 The precision of the REA system to resolve concentration differences ( $\Delta C_{REA}$ ) under field conditions was  
 257 derived from periods of reference sampling and based on the standard deviation of the residuals ( $\sigma_{\Delta C_{REA}}$ )  
 258 from orthogonal linear regression fitting of the conditional sampling channel reference concentrations  
 259  $C_{ref}^{\uparrow}$  vs.  $C_{ref}^{\downarrow}$  (Zhu et al., 2015b). The ambient air  $Hg^0$  concentration ( $C$ )-dependent relationship  
 260 ( $\sigma_{\Delta C_{REA}} = 0.057 + 0.016 \cdot C$ ,  $ng\ m^{-3}$ ) obtained from fitting data from all reference periods ( $N = 921$ )  
 261 was used to predict the method detection limit (MDL) for each flux observation. Using this criterion, the  
 262 proportion of  $Hg^0$  flux data above MDL was calculated for each campaign and listed in Table 1. Fifty-  
 263 seven percent of the  $Hg^0$  flux measurements were above MDL. For data integration, however, we choose to  
 264 use the complete dataset since average fluxes may otherwise be overestimated. The median of relative  
 265 uncertainty in individual 20-min  $Hg^0$  fluxes (derived by Eq. 5) is given for each campaign in Table 1. The  
 266 medians were constant (28 - 35%) across the campaigns. On a diurnal basis, relative uncertainty was  
 267 generally largest during the hours after sunrise, when sensible heat fluxes shifted direction and  $Hg^0$   
 268 concentration tended to fluctuate, cf. Zhu et al. (2015b).

### 269 3. 2 Environmental conditions

270 Meteorological quantities measured for each campaign during the study period are summarized in  
 271 Table 1. Air temperature and precipitation were within the range of mean values recorded for the site  
 272 over the past decade (Bao et al., 2014). However, specifically for the  $Hg^0$  flux measurement periods,  
 273 the precipitation frequency and total depth was sparse (in total 2.7 cm) and without notably influencing  
 274 soil moisture at any event.

275 In 2012, wheat started to elongate in late March and the peak in single-sided LAI (~2.4) appeared in early  
 276 May and then progressively declined as leaves in the under-layer turned yellow (Fig. 1). The weather  
 277 during campaign 1 was generally fair and moist with stable stratification predominant during night  
 278 ( $(z - d)/L = \zeta > 0.02$ , 78% of time,  $L$  is the Okuhkov length) while near-neutral (37% of time) and  
 279 unstable ( $\zeta < -0.02$ , 45% of time) conditions were frequent during daytime. The canopy was wet most  
 280 nights due to dew condensation while soil moisture initially at  $0.22\ m^3\ m^{-3}$  showed a declining trend over the

281 period (Fig. 4a). Campaign 2 was characterized by warm (mean air temperature 27 °C) and dry weather.  
282 Unstable conditions were predominant (93% of time) during daytime, partially leading to free convection  
283 ( $\zeta < -1$ ). The senescent canopy was wet only on occasional nights and topsoil layer was consistently dry  
284 ( $0.06 - 0.09 \text{ m}^3 \text{ m}^{-3}$ ). In the end of campaign, after wheat harvest, the field was flood irrigated (Fig. 4b).  
285 The main growing period for corn started after mid-July (DOY ~200) and maximum LAI ~3.7 was  
286 attained during second half of August (Fig. 1). The general meteorological condition during campaign 3  
287 was moist with periods of cloud cover and isolated rain showers. Low wind prevailed the vast majority of  
288 time (mean  $1.0 \text{ m s}^{-1}$ ) and the canopy remained wet for protracted periods (Fig. 4c). The lower turbulent  
289 exchange during those days is represented by low values of  $\sigma_w$  (mean:  $0.14 \pm 0.10 \text{ m s}^{-1}$ ), which has an  
290 impact on the REA flux (Eq. 1). As shown in Table 1, the mean  $\sigma_w$  for the period was lower than for any  
291 other campaign. Under the full-grown corn canopy, the topsoil remained moist over time ( $\sim 0.28 - 0.31 \text{ m}^3$   
292  $\text{m}^{-3}$ ).  
293 Hazy days with air temperature below zero were frequent during campaign 4 over frozen ground with  
294 dormant wheat. The site was under the influence by high-pressure systems and the haze reduced surface  
295 solar radiation, thereby leading to a more stable boundary layer with near-neutral or slightly stable  
296 ( $-0.02 < \zeta < 0.20$ ) atmospheric stratification dominated during daytime (81% of time) while air was  
297 prevailingly stable during night (79% of time). Snowfall occurred on Jan. 20 and ground was snow-  
298 covered towards the end of the period.  
299 In 2013, the peak in LAI for wheat was higher in magnitude ( $\sim 3.75$ ) and occurred already in late April.  
300 The weather conditions during campaign 5 featured moderate-to-strong wind speeds during daytime and  
301 relatively low air humidity without precipitation events. Mostly near-neutral or slightly unstable  
302 conditions were encountered during daytime (81% of time). During two campaigns, strong prevailing  
303 wind directions were present (Campaign 2 SW, 3 SSE), for another two there was a prevailing direction  
304 with a larger component of near counter-current flow (4, SSW – N; 5, SSW - NE) while the wind  
305 directions were more variable during campaign 3.

### 306 **3. 3 Ambient Hg<sup>0</sup> concentrations**

307 NCP is one of the heaviest impacted regions in China in terms of airborne Hg pollution and total Hg  
308 deposition fluxes (Wang et al., 2014b). Notwithstanding YCES is in a rural area, the surrounding NCP  
309 region has a high proportion of heavy and chemical industry clusters involving high energy consumption  
310 provided by foremost coal-fired power plants resulting in substantial Hg emissions to air (Zhang et al.,  
311 2013). Hg emission sources in rural districts include domestic and field burning of crop residue (Huang

312 et al., 2011) and illegal artisanal gold mining utilizing mercury amalgamation (AMAP/UNEP, 2013;  
313 Hall et al., 2014).

314 Throughout the measurement periods, concentrations of  $\text{Hg}^0$  were significantly variable (coefficient of  
315 variation: 27 - 33% for the individual campaigns). As listed in Table 1, the overall span of  $\text{Hg}^0$  observations  
316 ranged from background values infrequently below  $2 \text{ ng m}^{-3}$  to episodic peaks well above  $10 \text{ ng m}^{-3}$ .  
317 The overall average concentration of  $\text{Hg}^0$  for the measurement periods was  $4.3 \text{ ng m}^{-3}$ , which exceeded  
318 the highest seasonal average ( $3.5 \text{ ng m}^{-3}$ , summer) measured at a rural site in the Beijing region (Zhang  
319 et al., 2013) and that ( $2.7 \text{ ng m}^{-3}$ , winter) measured at the tip of Shandong peninsula (Ci et al., 2011).  
320 Mean values fell between  $3.4$  and  $5.2 \text{ ng m}^{-3}$  for the growing season individual campaigns (1-3, 5).  
321 Campaign 4 in January 2013 with a mean  $\text{Hg}^0$  concentration of  $6.2 \text{ ng m}^{-3}$  was characterized by  
322 prolonged and severe haze pollution episodes over the NCP region (Wang et al., 2014c). Available data  
323 show for Jinan municipal area, circa 50 km SE of the site, that hourly averaged fine particulate ( $\text{PM}_{2.5}$ )  
324 concentrations ranged between  $\sim 100 - 600 \mu\text{g m}^{-2}$  over the duration of Campaign 4 (Wang et al., 2014a).  
325 The  $\text{Hg}^0$  (YCES) and  $\text{PM}_{2.5}$  concentration (Jinan) time series have similar trends, implying that  $\text{Hg}^0$  at  
326 least in part share sources with air  $\text{PM}_{2.5}$  pollution. For January 2013, there is a contemporary  
327 atmospheric Hg data set collected in Qingdao (a major coastal city,  $\sim 340 \text{ km E.}$ ) averaging  $2.8 \pm 0.9 \text{ ng m}^{-3}$   
328 for  $\text{Hg}^0$  and  $245 \pm 174 \text{ pg m}^{-3}$  for particulate-bound Hg (Zhang et al., 2014) indicating that particulate-  
329 bound Hg (PBM) making up a substantial fraction of aerial Hg during the widespread winter haze.

330 All  $\text{Hg}^0$  concentration data sets showed positive skewness and kurtosis indicating a predominant  
331 influence of emission sources. In the panels of Fig. 2, the directionality of  $\text{Hg}^0$  concentration during the  
332 five campaigns was investigated by plotting pollution roses. In general,  $\text{Hg}^0$  showed no manifest  
333 dependence on ground wind direction over the sampling periods. However, during April 2013 (Fig.  
334 2e), the significantly lower  $\text{Hg}^0$  concentration associated with north-easterly wind directions was  
335 tentatively identified as air masses arriving from NE China/Russian Far-East via a slower passage over  
336 Bohai Sea (Fig. S1, Supplementary material).

337 Diurnal  $\text{Hg}^0$  concentration features for the each of the campaigns are shown in Fig. 3. Distinct profiles,  
338 which peaked during morning/daytime and reached a minimum at dusk/night-time were representative  
339 for most campaigns. During these periods,  $\text{Hg}^0$  displayed a significant negative correlation with  
340 atmospheric stability (Spearman's rank correlation,  $p < 0.01$ ). This daily variation pattern may reflect a  
341 limited importance of local ground-based  $\text{Hg}^0$  sources as no considerable level of  $\text{Hg}^0$  concentrations  
342 were observed to build up within shallow nocturnal boundary layer. First with the development of the

343 mixed layer, concentrations increased conceivably due to mixing-in of more Hg<sup>0</sup>-rich air from aloft.  
344 This is indicative of the intensity of regional Hg emission sources. In contrast, during the June campaign,  
345 episodes of elevated Hg<sup>0</sup> values occurred during series of nights associated with slightly stable conditions  
346 and low wind speeds (< 3 m s<sup>-1</sup>) but without a discernible dependence of wind direction (Fig. 4b). All  
347 of this suggests that the peaks derive from nocturnal in-field burning of crop residue occurring in the  
348 surrounding countryside during harvest season (Huang et al. 2011)..

### 349 **3. 4. Cropland-atmosphere exchange of Hg<sup>0</sup> and CO<sub>2</sub>**

350 In order to research the Hg<sup>0</sup> exchange between a cropland and the atmosphere, it is necessary to  
351 understand the seasonal variation in key environmental factors. For example, measured CO<sub>2</sub> net  
352 exchange provided valuable information about crop productivity and farmland ecosystem respiration  
353 over time. In Table 1, a statistical summary of Hg<sup>0</sup> and CO<sub>2</sub> net fluxes are given for the five sampling  
354 periods. Since both the distribution of Hg<sup>0</sup> fluxes and air concentrations deviated for several of the  
355 campaigns significantly from normality (Shapiro–Wilk test,  $p < 0.001$ ) median is supplied in Table 1 as  
356 an estimator of central tendency. Moreover, the statistical dependence between variables was assessed by  
357 non-parametric tests (Spearman's rank correlation, Table 2). Due to large spread in Hg<sup>0</sup> flux data, numerical  
358 smoothing was in this study performed on all data sets using a 9-point moving average (which corresponds  
359 to an interval of 3 hours) to reduce the variability and therefore allow for a better visual interpretation  
360 of diurnal variations (Cobos et al., 2002; Fritsche et al., 2008c). The associated time-series of smoothed  
361 Hg<sup>0</sup> and CO<sub>2</sub> flux are displayed in the composite Fig. 4. However, since the smoothing procedure  
362 introduces data manipulation, smoothed data are not used in any statistical treatments (such as  
363 correlation analysis, Table 2) or in the calculation of cumulative fluxes (shown in Fig. 4 and 8).

#### 364 **3. 4. 1 Average and ranges of fluxes for the different measurement periods**

365 Previous studies of the wheat - corn rotation farmland at YCES evinced it to be a significant sink of  
366 atmospheric CO<sub>2</sub> during the main growing seasons of winter wheat and corn (e.g. Li et al., 2006; Tong et  
367 al., 2014), which for our study overlap with campaign 1 (May) and 3 (August-September) and the end  
368 part of campaign 5 (late April). Using EC technique, a mean CO<sub>2</sub> uptake of 7.7, 6.2 and 6.7  $\mu\text{mol m}^{-2} \text{s}^{-1}$   
369 was determined for each of these sampling period (c.f. Fig. 4a, c & e). For the senescent wheat (campaign  
370 2), CO<sub>2</sub> uptake declined rapidly and in-turn ecosystem CO<sub>2</sub> respiration progressively gained more  
371 importance during day-time (with increased maximum temperatures) resulting in a mean CO<sub>2</sub> net  
372 exchange slightly below zero ( $-0.7 \mu\text{mol m}^{-2} \text{s}^{-1}$ ). The average Hg<sup>0</sup> above-canopy net flux was positive for  
373 the main growing season of winter wheat until harvest (April: 17.3, May: 26.7 and June: 16.5 ng m<sup>2</sup> h<sup>-1</sup>)

374 while slight dry deposition of  $\text{Hg}^0$  predominated over the field with a fully developed corn canopy  
375 (August - September, mean flux:  $-11.8 \text{ ng m}^{-2} \text{ h}^{-1}$ ). DFC measurements underneath the developed  
376 canopies show significant  $\text{Hg}^0$  soil emissions during daytime (Fig. 5). In more detail, mean air-soil  $\text{Hg}^0$   
377 fluxes were more strong evasive under the wheat canopy (May:  $39.9$  and June:  $31.5 \text{ ng m}^{-2} \text{ h}^{-1}$ ) than  
378 under the denser corn canopy (August-September:  $10.8 \text{ ng m}^{-2} \text{ h}^{-1}$ ). Sampling periods conducted over  
379 wheat in early growing stages were characterized by near-zero mean  $\text{CO}_2$  net flux (November:  $0.5$ ,  
380 January:  $-0.4$  and Early April:  $-0.7 \mu\text{mol m}^{-2} \text{ s}^{-1}$ ). As reported in Zhu et al. (2015a), collocated MM- and  
381 chamber flux measurement systems gauged unanimously positive net  $\text{Hg}^0$  flux (mean range:  $2.2 - 7.6$   
382  $\text{ng m}^{-2} \text{ h}^{-1}$ ) over the field during November.  $\text{Hg}^0$  fluxes during early April were also predominantly  
383 positive (mean:  $19.5 \text{ ng m}^{-2} \text{ h}^{-1}$ ) while the cumulative  $\text{Hg}^0$  flux was negative (mean:  $-11.6 \text{ ng m}^{-2} \text{ h}^{-1}$ ) for  
384 the winter period (Campaign 4) involving prolonged and severe haze air pollution episodes.

385 Irrespective of sampling period, extreme values in net  $\text{Hg}^0$  exchange (Table 1) were observed primarily  
386 during and after episodes when air with highly elevated  $\text{Hg}^0$  concentration advected over the fetch.  
387 Although highly dynamic, vertical fluxes of  $\text{Hg}^0$  were on an average substantially negative during such  
388 an event (cf. Fig. 4). On several occasions, the REA system gauged significant emission fluxes during  
389 the immediate period ensuing a major  $\text{Hg}^0$  dry deposition event. This temporal development also seen  
390 in other studies (Bash and Miller, 2007; Cobbett and Van Heyst, 2007) demonstrates the potential of  
391 deposited  $\text{Hg}^0$  to be promptly recycled to the atmosphere.

392 During most of the sampling campaigns, above-canopy  $\text{Hg}^0$  flux followed a discernible diurnal pattern  
393 with the absolute magnitude of the flux being largest during daytime periods and generally small at  
394 night (Fig. 3). However, the cycle of prevailing developed and weak atmospheric turbulence during  
395 day and night respectively was periodically disrupted by windy conditions extending into dark hours  
396 facilitating turbulent exchange (mostly encountered in winter and spring campaigns; Fig. 3g & i).

### 397 **3. 4. 2 $\text{Hg}^0$ flux patterns during main growing season**

398 Although the REA-measurements during the spring and summer campaigns indicate the wheat cropland  
399 to be a continual net source of atmospheric  $\text{Hg}^0$ , the correlation ( $\rho$ , Spearman's rank-order correlation  
400 coefficient) between  $\text{Hg}^0$  flux and other measured parameters varied significantly between the individual  
401 campaigns (Table 2). In contrast to a well-defined diurnal pattern in soil  $\text{Hg}^0$  efflux observed over the  
402 campaigns (Fig. 5), the average profiles in above-canopy  $\text{Hg}^0$  flux were non-uniform at the diurnal  
403 timescale. As shown in Fig. 3,  $\text{Hg}^0$  net fluxes above wheat canopies before canopy closure (April) and  
404 during senescence (June) were positive during day-time and from sunrise to noon respectively; while at

405 anthesis stage (May) composite flux data aligned to early afternoon minimum with mean deposition. The  
406 close agreement between the chamber and micrometeorological estimates during field inter-comparison  
407 (Zhu et al., 2015a) prompted us in the present study to interpret  $\text{Hg}^0$  in-canopy fluxes from the difference  
408 between REA- and DFC-observations despite the fact that the methods covering different spatial scales.  
409 For two of the campaigns (1 and 3) during the final vegetative stage of corn and wheat, ground and  
410 above-canopy  $\text{Hg}^0$  fluxes displayed inversed daytime courses with near mid-day maximum and minimum  
411 respectively (Fig. 6). These data supported that the active growing and developed cereal canopies acted as  
412 a daytime sink of  $\text{Hg}^0$  and at least in part were able to offset the concurrent emission from ground  
413 surfaces. During these periods, above-canopy  $\text{Hg}^0$  flux was negatively correlated with air  $\text{Hg}^0$   
414 concentration and positively correlated with  $\text{CO}_2$  flux (Table 2). To examine temporal variability of fluxes  
415 in more detail, specific observations for campaigns 1 and 3 are presented in succession below.

416 During day-time for a series of days with significant  $\text{CO}_2$  uptake (May, 4 - 9),  $\text{Hg}^0$  dry deposition was  
417 predominant (Fig. 4a). From the mid of the campaign and onwards, periods of above-canopy  $\text{Hg}^0$   
418 emission become more frequent than deposition during daytime. Such a trend in above-canopy  $\text{Hg}^0$   
419 flux is not reflected in ground  $\text{Hg}^0$  flux and may therefore be related to in-canopy  $\text{Hg}^0$  source/sink  
420 characteristics. During the May period, the mean  $\text{Hg}^0$  net fluxes were negative for the hours coincident  
421 with the diurnal maximum in  $\text{Hg}^0$  concentration (Fig. 3a, b). Given the indication for  $\text{Hg}^0$  uptake by the  
422 canopy when ambient concentrations were elevated, lower  $\text{Hg}^0$  concentrations during the second phase  
423 of the period together with expected decline in  $\text{Hg}^0$  uptake with growth progression (Du and Fang,  
424 1983) may explain the result. The principal diel period of  $\text{Hg}^0$  deposition did not concur with the peak  
425 canopy conductance during morning hours, suggesting that foliar uptake of  $\text{Hg}^0$  is not limited by periods  
426 of ample stomatal conductance. Instead, maximum mean  $\text{Hg}^0$  deposition during campaign 1 appeared in  
427 the early afternoon, which is in concert with that of  $\text{O}_3$  observed in a contemporary study over wheat at  
428 YCES (Zhu et al., 2015c). Daytime deposition of  $\text{Hg}^0$  were also gauged over fully leafed graminaceous  
429 plant canopies by Lee et al. (2000) and Fritsche et al. (2008c) and attributed to plant biological activities  
430 such as photosynthesis. Since net  $\text{Hg}^0$  fluxes were bi-directional with atmospheric  $\text{Hg}^0$  concentrations  
431 appearing to play a significant role in controlling flux, the response may be interpreted with the concept of  
432 an  $\text{Hg}^0$  canopy compensation point (Bash and Miller, 2009; Ericksen and Gustin, 2004; Hanson et al.,  
433 1995; Poissant et al., 2008). The apparent compensation point calculated from linear regression ( $r = -$   
434  $0.32$ ,  $p < 0.001$ ) was at  $\sim 5.3 \text{ ng m}^{-3}$  for May. However, it is clear that the parameter is a composite term,  
435 which is influenced by component sources/sinks within the canopy as well as at ground (Wright and  
436 Zhang, 2015). In particular, air-soil  $\text{Hg}^0$  flux observations were overall not linked to a compensation point

437 behavior ( $r = 0.07$ ,  $p = 0.22$ ) but at large governed by the effect of global radiation and soil temperature  
438 (explaining 68.3% of variance in the total data, stepwise multivariate regression).

439 Without much day-to-day variation,  $\text{Hg}^0$  dry deposition occurred during daytime over the entire campaign  
440 3 (Fig. 4c). At the diurnal timescale,  $\text{Hg}^0$  flux shows a shallow minimum ( $\sim -40 \text{ ng m}^{-2} \text{ h}^{-1}$ ) over corn just  
441 before noon-time coinciding with the peak in atmospheric  $\text{Hg}^0$  concentration (Fig. 3e, f). Under the dense  
442 corn canopy structure the magnitude of daytime  $\text{Hg}^0$  efflux from soil was on an average a factor  $\sim 3$  lower  
443 compared to that within the wheat canopy (Fig. 5) and may attributed to a combination of lower light  
444 transmission to ground and profoundly dampened diurnal courses in surface soil temperature (c.f. Fig. 4).  
445 In addition, the entirely moist surface soil may restrain  $\text{Hg}^0$  evasion by reducing its mobility through the soil  
446 profile (Schlüter, 2000). The divergence in dynamic scale of the diurnal  $\text{Hg}^0$  fluxes observed at each  
447 vertical level (Fig. 6) indicate that corn with a higher above-ground biomass is a weaker  $\text{Hg}^0$  sink (per leaf  
448 area) than wheat as previously been inferred from controlled experiments (Browne and Fang, 1983; Niu  
449 et al., 2011).  $\text{Hg}^0$  uptake in cereals is plausibly associated with the enzymatic conversion of  $\text{Hg}^0$  to  $\text{Hg}^{\text{II}}$   
450 species within the foliar cavity (Du and Fang, 1983). Transient  $\text{Hg}^0$  foliar uptake during campaign 1 and 3  
451 (encompassing similar meteorological conditions, Table 1) as calculated from the integrated imbalances  
452 between ground and above-canopy flux during daytime was at  $0.17 \pm 0.08$  and  $0.46 \pm 0.32 \mu\text{g m}^{-2}$  leaf  
453 area  $\text{day}^{-1}$ , respectively. The apparent canopy compensation point of  $\sim 3.6 \text{ ng m}^{-3}$  is lower than derived for  
454 the wheat during campaign 1. The discrepancy may in part be explained by the greater positive responses in  
455  $\text{Hg}^0$  uptake to both light and temperature for wheat ( $\text{C}_3$  plant) compared to corn ( $\text{C}_4$  plant) reported by  
456 Du and Fang (1982). Essentially, above-canopy  $\text{Hg}^0$  dry deposition during campaign 1 was confined to  
457 the mid-day, which was characterized by elevated  $\text{Hg}^0$  in addition to high temperatures and irradiance.  
458 Individually all these parameters have been reported to significantly promote  $\text{Hg}^0$  uptake by wheat (Du  
459 and Fang, 1982) and in close association their combined effect appear required to offset the substantial  
460 ground emission of  $\text{Hg}^0$ .

461 The dynamics of  $\text{Hg}^0$  flux over wheat during April and June campaigns with net  $\text{Hg}^0$  emission  
462 prevailing during daytime and small nocturnal median fluxes suggests a limited capacity of the canopy  
463 to recapture  $\text{Hg}^0$  efflux from ground. Being a  $\text{C}_3$ -plant, the foliar  $\text{Hg}^0$  uptake is susceptible to light and  
464 temperature conditions (Du and Fang, 1982). Under sub-optimal conditions with low leaf temperature  
465 present in April (mean air temperature  $9.8 \text{ }^\circ\text{C}$ ), resistances are accordingly increased and rates of  $\text{Hg}^0$   
466 net uptake by wheat foliage are presumably lower. Over the senescent canopy,  $\text{Hg}^0$  flux showed  
467 frequently a profound short-term temporal variability overlaid on a trend towards higher emission rates  
468 (Fig. 4b). The changing physiological properties of wheat occurring after the onset of senescence



469 (Grossman-Clarke et al., 1999) together with crop water stress might account for the disparity between  
470 early phase-May and June day-time Hg<sup>0</sup> canopy-scale fluxes. A prominent feature of the average diurnal  
471 pattern of latter fluxes is the more largely Hg<sup>0</sup> net emission during the early morning (Fig. 3c). The  
472 temporary low Hg<sup>0</sup> ground evasion (mean:  $9.9 \pm 25.0 \text{ ng m}^{-2} \text{ h}^{-1}$ ) indicating that the episodic Hg<sup>0</sup>  
473 emissions stem from above-ground (cf. Fig. 5b). Owing to the dry conditions, we may exclude the  
474 possibility of Hg<sup>0</sup> deriving from evaporation of dew-wetted foliar surfaces. It is more likely that the  
475 morning peak in Hg<sup>0</sup> flux results from canopy release of Hg<sup>0</sup> (following the timing of maximum values of  
476  $g_c$  and there is an overall positive correlation between flux and  $g_c$ ,  $\rho = 0.23$ ,  $p < 0.001$ ) and venting of the  
477 canopy by increasing wind speeds. For wheat, there is observational evidence for transpiration flow  
478 transport of Hg<sup>II</sup> species (Khozhina et al., 2001), which may become chemical reduced when reaching  
479 mesophyll through electron transfer schemes from the anti-oxidative defense system via ascorbate and  
480 potentially emitted as Hg<sup>0</sup> (Battke et al., 2005). In association with rapid decline in canopy transpiration  
481 (Table 1) and enzymatic-mediated Hg<sup>0</sup> oxidation in mature wheat (Du and Fang, 1983), our result suggests  
482 a capacitance of Hg<sup>0</sup> storage within the substomatal cavity which being released when the stomata once  
483 open. The fact that the morning peak in Hg<sup>0</sup> emission occurs albeit elevated Hg<sup>0</sup> concentration in air  
484 renders more credibility to this hypothesis.

### 485 **3. 4. 3 Hg<sup>0</sup> flux patterns during non-growing season**

486 For the periods with near-zero CO<sub>2</sub> net flux indicative of non-significant plant growth, there is a  
487 marked difference between overall Hg<sup>0</sup> net emission occurring during late fall and early spring and net  
488 deposition during mid-winter (Tukey-Kramer test,  $p < 0.01$ ). The experimental field with emerging  
489 wheat was relatively dry during these sampling periods (soil moisture content at 5 cm depth of 0.06 -  
490  $0.17 \text{ m}^3 \text{ m}^{-3}$ ). Without a significant canopy cover, the farmland-atmosphere Hg<sup>0</sup> net exchange gauged  
491 during these periods would essentially derive from soil fluxes. In correspondence to air-soil Hg<sup>0</sup> fluxes  
492 measured within the developed canopies during warmer seasons (Fig.5), field-scale Hg<sup>0</sup> fluxes were  
493 during November associated with an average diurnal profile featuring maximum emission near mid-  
494 day ( $\sim 40 \text{ ng m}^{-2} \text{ h}^{-1}$ ; Fig. 9 in Zhu et al., 2015a). The higher mean Hg<sup>0</sup> fluxes observed during early  
495 April compared to November (Section 3. 4. 1) may in part be linked to warming soil temperatures  
496 during the former period (mean: 10.9 vs. 5.3 °C) given the similar level of surface soil moisture. Numerous  
497 studies have shown that surface soil temperature has a strong influence on relatively dry soil Hg<sup>0</sup> efflux  
498 due to its role in enhancing volatilization (Carpi and Lindberg, 1997; Gustin et al., 1997; Poissant et al.,  
499 2004; Xiao et al., 1991). In the current study, Hg<sup>0</sup> dry deposition occurred more frequently than emission

500 at daytime (Fig. 3g) during the winter period with sub-zero ground temperatures (Fig. 4d). In contrast  
501 to the late fall and early spring period,  $\text{Hg}^0$  fluxes were in winter significant negatively correlated with  
502  $\text{Hg}^0$  concentration ( $\rho = -0.35$ ,  $p < 0.001$ ). A better part of the cumulative  $\text{Hg}^0$  flux occurred in a few  
503 distinct periods (Jan. 13 - 15; 22 - 24, Fig. 4d) whereas for the remainder there was small day-to-day  
504 variation. These periods were characterized by more extreme values in  $\text{Hg}^0$  and  $\text{PM}_{2.5}$  air pollution  
505 (Section 3. 3). In addition, snowfall samples collected had elevated Hg concentrations (Section 3. 5)  
506 suggesting enrichment by scavenging of Hg bound to aerosols. It should be noted that  $\text{Hg}^0$  fluxes  
507 reported here for winter could represent extremes rather than average seasonal conditions. As can be  
508 seen in Fig. 4d, events of substantial  $\text{Hg}^0$  dry deposition were in general followed by a period of net  
509 emission suggesting frozen surfaces to be a transient sink for atmospheric  $\text{Hg}^0$ . Cobbett and Van Heyst  
510 (2007) also found that elevated concentrations of  $\text{Hg}^0$  ( $> 10 \text{ ng m}^{-3}$ ) resulted in highly dynamic net  $\text{Hg}^0$   
511 fluxes over agricultural soil below  $0^\circ\text{C}$  with dry deposition shifting to emission whereas net exchange  
512 were concomitantly low under ambient conditions.

#### 513 **3. 4. 4 Flux responses to abrupt changes in environmental conditions**

514  $\text{Hg}^0$  flux data were examined for discernible response to abrupt changes in environmental conditions due  
515 to agricultural management operations (e.g. tilling and irrigation) and precipitation as such events have  
516 previously been linked to increases in  $\text{Hg}^0$  emission from soils (Bash and Miller, 2007; Baya and Van  
517 Heyst, 2010; Gillis and Miller, 2000; Lindberg et al., 1999). In June 2012, while the topsoil was  
518 substantially dry ( $\sim 0.06 \text{ m}^3 \text{ m}^{-3}$ ), wheat harvest (the fields making up our primary fetch) started on June 23  
519 and was completed the next following day. The harvesting had no discernible boosting effect on  $\text{Hg}^0$   
520 concentration in air while  $\text{Hg}^0$  air-surface exchange showed significant bi-directional fluctuations during  
521 this period yielding a surplus of  $\text{Hg}^0$  emission (Fig. 4b). In turn, field flood irrigation was conducted on  
522 June 26 starting from the southern end of the field south of the eddy tower (distance  $\sim 130 \text{ m}$ ). The  
523 flooding of southern field was completed soon after noon-time (indicated by the ramp in soil moisture  
524 measured near the flux tower, Fig. 7). During most of this irrigation period the REA flux footprint fall  
525 outside the primary area. However, as wind gradually turned towards southerlies (and increasing from  $\sim 2$   
526 to  $\sim 4 \text{ m s}^{-1}$ ), the integrated flux signal derived increasingly from wetted field surfaces with good  
527 representativeness commencing at noon and following few hours (90% isopleth footprints predicted at  
528  $107 \pm 43 \text{ m}$  during this period, concerning models employed for this purpose cf. Sommar et al. 2013b).  
529 As seen in Fig. 7,  $\text{Hg}^0$  and water vapor fluxes jointly show enhancement after the wind transition  
530 indicating volatilization of  $\text{Hg}^0$  from soils occurred in response to field irrigation. After initial spike-like

531 features ( $>300 \text{ ng m}^{-2} \text{ h}^{-1}$ ), there is a decline in  $\text{Hg}^0$  flux over the time the irrigated field was up-wind the  
532 measurement system (until  $\sim 17:30$ ). Similar observations have been made from field and controlled  
533 laboratory experiments, where prompt and substantial release of  $\text{Hg}^0$  from soils has been observed  
534 following precipitation/irrigation provided the soil initially was quite dry (Bahlmann et al., 2004;  
535 Lindberg et al., 1999; Song and Van Heyst, 2005). Possible causes to the observed pattern include  
536 physical displacement of soil pore air enriched in  $\text{Hg}^0$  and desorption of  $\text{Hg}^0$  loosely bound onto surfaces  
537 as water percolates into the soil (Lindberg et al., 1999). Over the course of the rest of campaign 2, the  
538 magnitude and variability in  $\text{Hg}^0$  flux was substantially lower (minor emission flux predominant) than  
539 before irrigation (Fig. 4b). In correspondence, Schroeder et al. (2005) found that persistent rain and high  
540 soil moisture contents inhibit Hg evasion from soils, which could be linked to restrictions in the  
541 replenishment of  $\text{Hg}^0$  towards the soil surface due to low diffusivity through water-filled micropores  
542 (Schlüter, 2000). Overall, precipitation events were scarce during the flux measurement periods. During  
543 campaign 3, two substantial precipitation events occurred on Sep. 2 and 7 (c.f. Fig. 4c) but none of the  
544 events yielded any discernible enhancement in  $\text{Hg}^0$  emission (unanimously gauged by REA and DFC).  
545 As aforementioned, surface soil was relatively moist during this period, which may acted as a controlling  
546 factor (Song and Van Heyst, 2005).

### 547 **3. 5. Wet deposition Hg fluxes and mature crop foliar Hg concentrations**

548 For the study period with a precipitation depth of 51 cm, the volume weighted mean THg concentration in  
549 precipitation was  $17.2 \text{ ng L}^{-1}$  corresponding to a cumulated wet deposition flux of  $8.8 \mu\text{g Hg m}^{-2}$  (Fig. 8).  
550 Maximum concentrations ( $-113.3 \text{ ng L}^{-1}$ ) were detected in event precipitation during winter. However,  
551  $\sim 65\%$  of the THg wet deposition flux for the period occurred during the summer months due to the  
552 largely asymmetric pattern in annual precipitation (c.f. Fig. 8 and Table S1 in the supplementary  
553 information). The large temporal variability and range of concentrations among the samples (Table S1)  
554 corresponds well with observations at rural sites influenced by strong regional Hg combustion sources  
555 (Keeler et al., 2006; Schwesig and Matzner, 2000).

556 THg content in mature corn and wheat foliage associated with stands of a dry leaf mass density of  $\sim 0.5 \text{ kg}$   
557  $\text{m}^{-2}$  was determined to  $36.4 \pm 3.1$  ( $n = 3$ ) and  $122.9 \pm 13.9 \text{ ng g}^{-1}$  dry weight ( $n = 6$ ) respectively. The  
558 observed foliar Hg level is comparable with the results obtained from controlled exposure of corn and  
559 wheat to elevated  $\text{Hg}^0$  concentrations in air (Niu et al., 2011). The higher Hg accumulation in wheat  
560 compared to corn foliage aligns well with the differential  $\text{Hg}^0$  uptake inferred from  $\text{Hg}^0$  flux measurements  
561 (Section 3. 4. 2). Furthermore, compartmentalized Hg analysis of mature corn plants shows the Hg content

562 increased in the order root ( $5.7 \pm 1.1 \text{ ng g}^{-1}$ ,  $n=5$ ) < stem ( $12.8 \pm 3.5 \text{ ng g}^{-1}$ ,  $n=5$ ) < foliage, which is  
563 indicative that vegetative uptake of airborne  $\text{Hg}^0$  is primarily retained in cereal crop leafage. Worth to  
564 notice is also that the THg content in our wheat foliage samples exceeding the maximum level ( $110 \text{ ng g}^{-1}$   
565 dry weight) in animal feeding material (forage) issued by the European Union (EC, 2002). In addition, a  
566 survey of heavy metals in wheat and corn crops grown in the study area by Lin et al. (2010) has revealed Hg  
567 content in wheat grain at levels proximate to or prevalently exceeding the Chinese tolerance limit for food  
568 ( $20 \text{ ng g}^{-1}$  dry weight.).

## 569 **4. Discussion**

### 570 **4. 1 $\text{Hg}^0$ exchange between atmosphere and grain croplands**

571 Measurements over the wheat-corn rotational cropland in NCP show that each of vegetation and soil  
572 exchange processes are important in defining net  $\text{Hg}^0$  fluxes. The emergence of a canopy layer creates  
573 a sink for atmospheric Hg while the canopy cover reduces the potential of underlying soil to act as an  
574  $\text{Hg}^0$  source. Our data also impart that besides vegetation density (LAI) and the physical plant structure,  
575 the type of cultivated cereal crop has an effect on  $\text{Hg}^0$  gas exchange by species-specific foliage uptake  
576 rates. Nevertheless, chamber measurement made here evinced that ground  $\text{Hg}^0$  emissions within  
577 developed crop canopies are substantial in the warmer season. Regardless of growing stage,  $\text{Hg}^0$  uptake  
578 by wheat canopies is not equal to cumulatively offset the  $\text{Hg}^0$  efflux from ground surfaces (April - June  
579 mean  $\text{Hg}^0$  net flux:  $20.0 \text{ ng m}^{-2} \text{ h}^{-1}$ ). Flux data available in this study over corn indicate that the full-  
580 grown, dense canopy can dominate the  $\text{Hg}^0$  exchange process resulting in daytime net deposition. For  
581 the early growing stages of corn not measured in this study, MM flux measurements by (Cobos et al.,  
582 2002) and (Baya and Van Heyst, 2010) over non-contaminated soils (THg:  $\sim 25$  and  $\sim 50 \text{ ng g}^{-1}$   
583 respectively) quantified net  $\text{Hg}^0$  emission to prevail (mean flux:  $9.7$  and  $15.2 \text{ ng m}^{-2} \text{ h}^{-1}$ ). Considering  
584 all the micro-meteorological  $\text{Hg}^0$  flux data set collected over the full year 2012 - 2013 study period (using  
585 REA during campaign 1 - 5 and MBR during IC in November, Zhu et al., 2015a) yield an overall mean  
586  $\text{Hg}^0$  evasion flux of  $7.1 \text{ ng m}^{-2} \text{ h}^{-1}$  accounting for nearly 5700 individual  $\text{Hg}^0$  flux observations. Although,  
587 there is substantial periods over the 2012 - 2013 study when flux measurements not were conducted, it  
588 appears that the wheat-corn rotational cropland investigated constitute a net source of atmospheric  $\text{Hg}^0$   
589 on an annual basis. Any definite estimate of annual  $\text{Hg}^0$  flux is however not feasible due to the large  
590 uncertainty inherent in such an attempt at extrapolation. Before a robust estimate can be constructed, other  
591 factors such as the degree of inter-annual variability must also be considered. Nevertheless, the direction  
592 and magnitude of the mean  $\text{Hg}^0$  flux measured at our site agree well with that ( $6.3 \text{ ng m}^{-2} \text{ h}^{-1}$ ) reported by

593 Baya and Van Heyst (2010) for Hg<sup>0</sup> exchange over a soybean - corn cropland (Nov. - April and June). For  
594 croplands, the study of Baya and Van Heyst (2010) is the only one found in the literature of comparable  
595 temporal extent with our study. Although spanning across seasons, their reported Hg<sup>0</sup> flux data however  
596 only marginally target seasons with substantial crop canopy closure. There are growing seasonal studies of  
597 Hg<sup>0</sup> net exchange over biomes predominantly vegetated by stands of non-cereal graminaceous plants. Lee et  
598 al. (2000) reported for a fetch of growing salt meadow cord grass a trend from net emission during the  
599 period before complete leaf-out (mean: 1.8 ng m<sup>-2</sup> h<sup>-1</sup>) to predominant dry deposition during full foliage stage  
600 (mean: -3.3 ng m<sup>-2</sup> h<sup>-1</sup>). In correspondence to our study, Smith and Reinfelder (2009) observed significant  
601 day-time Hg<sup>0</sup> deposition over a full-grown canopy (*Phragmites australis*) coinciding with elevated ambient  
602 air concentrations.

603 The magnitude of average mid-day Hg<sup>0</sup> dry deposition over full-grown wheat and corn (Fig. 6) could be  
604 reproduced using a single-layer modeling approach (Wesely and Hicks, 1977) with a total leaf conductance  
605 parameterization to Hg<sup>0</sup> according to Lindberg et al. (1992) and input of average mid-day observations of  
606 conductances  $g_a$  (3.5 cm s<sup>-1</sup>) and  $g_c$  (2.1 cm s<sup>-1</sup>) together with  $C$  (4.1 - 6.6 ng m<sup>-3</sup>). Associated cereal foliar  
607 Hg<sup>0</sup> uptake rates estimated by combined REA- and DFC-measurements compares in magnitude (~7 - 19 ng  
608 m<sup>-2</sup> leaf area h<sup>-1</sup>) favorably with observations for aspen foliage in controlled gas-exchange systems operated  
609 at moderately elevated Hg<sup>0</sup> concentrations (Ericksen and Gustin, 2004; Ericksen et al., 2003). The periods  
610 with consistent daytime imbalances between above- and under-canopy flux during early phase of campaign  
611 1 (wheat) and campaign 3 (corn) explain up to ~20% and ~50% of the quantity of Hg accumulated by the  
612 mature foliage of wheat and corn respectively. This indicates that a relatively high contribution of the  
613 mercury load to the cereal occurring during its final vegetative stage. In many circumstances, our  
614 micrometeorological flux estimates appear better suited to address the magnitude of the net cropland-  
615 atmosphere exchange and not ideal in combination with DFC for constraining vegetative Hg<sup>0</sup> uptake as  
616 the ground surface is the major source of Hg<sup>0</sup> emission. Nonetheless, controlled experiments (Niu et al.,  
617 2011) envisaged on-going assimilation of atmospheric Hg<sup>0</sup> by winter wheat during its extensive period of  
618 leaf production for which we have limited REA and DFC flux data coverage.

#### 619 **4. 2 Implications for estimation of a local Hg budget**

620 Besides Hg<sup>0</sup> air-surface exchange focused on in this study, Hg input through dry deposition of other  
621 atmospheric Hg forms (gaseous oxidized mercury (GOM) and particulate-bound mercury (PBM)) and  
622 bulk THg wet deposition are potentially important pathways in the local Hg cycle. Projecting the scale  
623 of THg wet deposition to Hg<sup>0</sup> soil emission predominant over the vast majority of year (Fig. 8), it is

624 unlikely that wet deposition even on a short-term basis could support for the magnitude of volatilization  
625 observed at YCES. Given the top soil horizon has a uniform and low THg content, it is also unlikely  
626 that its inherent Hg pool can sustain substantial losses to atmosphere via Hg<sup>0</sup> volatilization without  
627 continual replenishment. We therefore hypothesize that Hg input from a combined removal of atmospheric  
628 GOM and PBM constitute the major deposition pathway to this site. High ratios of PBM<sub>2.5</sub> (Hg bound  
629 to PM<sub>2.5</sub>) to GOM as well as of PBM<sub>2.5</sub> to Hg<sup>0</sup> are characteristic for atmospheric Hg in the NCP region  
630 (Zhang et al., 2013). In China, there is a paucity of observational Hg dry deposition studies. However, a  
631 high dry-to-wet Hg deposition ratio has been inferred from studies of Chinese forested ecosystems (Fu  
632 et al., 2015; Wang et al., 2009). Predicted total Hg deposition to the site area using simulations by the  
633 GEOS-Chem model is elevated and of the order 80 - 100 µg m<sup>-2</sup>yr<sup>-1</sup> (Wang et al., 2014b), which would  
634 in theory quantitatively allow for a reasonably high Hg<sup>0</sup> efflux from agricultural soils in the NCP region.  
635 This presupposes that a significant portion of Hg<sup>II</sup> species deposited to the ecosystem is labile towards  
636 reduction to Hg<sup>0</sup>, which in succession should be extensively re-emitted back to the atmosphere. In the  
637 literature, there is support for that contemporary deposited Hg to larger extent than the ambient Hg pool  
638 in terrestrial ecosystems is recycled to the atmosphere via surface photo-reduction and re-volatilization  
639 (Eckley et al., 2013; Ericksen et al., 2005; Graydon et al., 2006; Graydon et al., 2012; Hintelmann et  
640 al., 2002). The observed abrupt pulse in Hg<sup>0</sup> emissions from dry soil in response to flood irrigation  
641 (Section 3.4.4) suggests the seasonal presence of an ample pool of Hg<sup>0</sup> in the upper soil horizon. Soil  
642 characteristics present at YCES such as low level of organic matter (Edwards and Howard, 2013; Fu et  
643 al., 2012; Sigler and Lee, 2006), clayey components (Biester et al., 2002) and high alkalinity (Landa,  
644 1978; Xin and Gustin, 2007; Yang et al., 2007) appear to facilitate Hg<sup>0</sup> formation, which in association  
645 with prevalent residual porosity allows for Hg<sup>0</sup> mobility towards the soil-air interface and losses to air. The  
646 differential magnitude of Hg<sup>0</sup> soil efflux measured under developed canopies with moist and dry soil  
647 respectively indicates that the combined level of precipitation/irrigation is one of the most important  
648 seasonal variables that control the magnitude of Hg<sup>0</sup> emission from ground at the site.

## 649 **5. Conclusions**

650 In this paper, we present a broad seasonal record of Hg<sup>0</sup> net flux observations during 2012 - 2013 over a  
651 wheat-corn inter-cropping field located in the North China Plain. Our work appears to be the first that  
652 investigated Hg<sup>0</sup> gas-exchange along the essential growing phases of a managed cropland from sowing  
653 to the crop maximum development. Our initial hypothesis was that the elevated atmospheric Hg<sup>0</sup>  
654 concentrations in the NCP region would promote depositional Hg<sup>0</sup> fluxes over cropland ecosystems

655 provided with low native soil Hg content. However, during the wheat growing season covering  $\sim 2/3$  of  
656 the year at the site, we observed net  $\text{Hg}^0$  emission prevailing during periods of active plant growth until  
657 canopy senescence (April - June mean  $\text{Hg}^0$  net flux:  $20.0 \text{ ng m}^{-2} \text{ h}^{-1}$ ). The result can be explained by a  
658 dominance of  $\text{Hg}^0$  emissions from ground surfaces during daytime in relation to  $\text{Hg}^0$  uptake by overlying  
659 foliage regardless of canopy cover. In comparison to corn, the developed wheat stand provide limited  
660 canopy cover and had less effect in attenuating light and dampening the evolution of high surface soil  
661 temperatures which promoted elevated daytime soil  $\text{Hg}^0$  efflux (daily mean maximum fluxes  $>100 \text{ ng m}^{-2}$   
662  $\text{h}^{-1}$ ) during warm seasons. Only in the fully leafed period (anthesis stage), wheat canopy shows high  
663 capacity to recapture  $\text{Hg}^0$  emissions from the soil during the day.  $\text{Hg}^0$  efflux under the corn canopy near  
664 peak LAI was on an average a factor of three lower and the temporal dynamics of net  $\text{Hg}^0$  flux above  
665 the canopy indicated the cropland to be a weak  $\text{Hg}^0$  sink during this period. Measurements near peak LAI  
666 of wheat and corn suggest  $\text{Hg}^0$  exchange following the concept of a canopy compensation point (at  
667  $\sim 5.3$  and  $\sim 3.6 \text{ ng m}^{-3}$  respectively). In response to agricultural management by flood irrigation, a peak  
668 of enhanced  $\text{Hg}^0$  emission was recorded from the initially dry field as an effect of expulsion of soil gas  
669 rich in  $\text{Hg}^0$  by infiltrating water. In conclusion, it appears that the wheat-corn rotational cropland  
670 investigated constitute a net source of atmospheric  $\text{Hg}^0$  on an annual basis. In addition, the practice of  
671 in-field burning of crop residue in the NCP seasonally release substantial amount of  $\text{Hg}^0$  to air from the  
672 plant material and burnt soil. Due to the imbalance between THg wet deposition ( $\sim 8.8 \mu\text{g m}^{-2} \text{ yr}^{-1}$ ) at  
673 YCES and gaseous loss by  $\text{Hg}^0$  soil volatilization predominant over the vast majority of year, it is  
674 suggested that dry deposition of other forms of airborne Hg (GOM and PBM) would constitute the  
675 major pathway of local Hg input. Gradual reduction of previous deposited atmospheric Hg promoted  
676 by warming temperature and solar load may explain the summer season observation of a discernible  
677  $\text{Hg}^0$  soil pool. Future experimental work should besides net canopy-scale and canopy-floor  $\text{Hg}^0$  fluxes  
678 also focus on elucidating foliage Hg exchange processes by in-canopy measurements.

## 679 **Acknowledgements**

680 This research was supported by the State Key Laboratory of Environmental Geochemistry, the 973  
681 Program (2013CB430002), the National Science Foundation of China (41373056, 41030752) as well  
682 as by the Chinese Academy of Sciences through an instrument development program (YZ200910).  
683 The technical staff of YCES is greatly appreciated for the facilities and infrastructure kindly made  
684 available to the authors.

686 **Table 1.** Summary of turbulent Hg<sup>0</sup> fluxes measured by REA technique, micrometeorological  
 687 parameters measured by EC and auxiliary meteorological and environmental observations (presented  
 688 as 20-min averages) during the five campaigns.

Variable	Unit	1 (May 2-18, 2012)		2 (June 12 - 29, 2012)		3 (Aug. 29 - Sept. 17, 2012)		4 (Jan. 12 - 24, 2013)		5 (April 1 - 24, 2013)	
		Wheat, ~65-70cm, LAI ~2.4 - 1.0		Wheat, ~70 cm, LAI < 1.0		Corn, ~255 cm, LAI ~3.6 - 2.7		Wheat, ~10 cm, LAI ~0.4		Wheat, ~30-35cm, LAI ~1.8 - 3.6	
		Range	Mean (median)	Range	Mean (median)	Range	Mean (median)	Range	Mean (median)	Range	Mean (median)
Air temperature	°C	9.7 - 30.1	20.4 (20.0)	13.4 - 38.1	26.9 (26.4)	8.5 - 33.7	21.1 (21.3)	-13.1 - 6.6	-2.2 (-2.3)	0.0 - 22.8	9.8 (9.8)
Soil temperature	°C	14.7 - 26.3	19.9 (19.4)	18.9 - 32.9	26.6 (26.7)	17.5 - 26.7	22.0 (21.8)	-6.6 - 0.0	-1.5 (-0.8)	1.5 - 22.3	10.9 (10.4)
Air humidity	%	1.7 - 99.7	84.3 (90.7)	18.1 - 99.3	59.1 (59.9)	33.7 - 99.8	85.2 (92.4)	52.7 - 99.8	90.7 (95.1)	34.3 - 100	73.0 (74.5)
Global radiation	W m <sup>2</sup>	0.6 - 1065.6	249.7 (54.4)	0.6 - 956.9	206.8 (45.6)	0.6 - 1010.6	176.2 (11.9)	0.6 - 428.1	57.1 (0.6)	0.6 - 890.6	158.4 (7.5)
Leaf wetness	%	3.5 - 100.0	42.8 (19.4)	2.4 - 100.0	19.9 (5.3)	5.9 - 100.0	59.4 (91.9)	5.9 - 100.0	89.5 (100.0)	2.4 - 100	37.0 (8.2)
Precipitation	mm	[—]	0.2	[—]	1.2	[—]	13.6	[—]	4.0	[—]	8.0
PAR photon flux	μE	1.2 - 1956.2	449.6 (91.6)	1.2 - 1826.2	414.0 (106.2)	1.2 - 2021.2	350.3 (26.2)	1.2 - 778.7	104.5 (1.2)	1.2 - 1621	298 (13.7)
Soil water content	(%vol)	10.4 - 21.6	14.6 (14.0)	5.5 - 36.6	11.1 (8.1)	28.0 - 30.5	29.0 (28.9)	4.6 - 14.6	6.4 (6.1)	5.3 - 8.8†	6.3 (6.1)†
Wind speed	ms <sup>-1</sup>	0.01 - 4.08	1.32 (1.22)	0.01 - 7.24	2.00 (1.74)	0 - 6.08	1.00 (0.86)	0.01 - 7.61	2.02 (1.67)	0.00 - 8.91	2.74 (2.60)
Friction velocity	ms <sup>-1</sup>	0.01 - 0.54	0.16 (0.15)	0.01 - 0.71	0.18 (0.17)	0 - 0.61	0.13 (0.10)	0.01 - 0.75	0.15 (0.12)	0.00 - 1.59	0.23 (0.19)
σ <sub>w</sub>	ms <sup>-1</sup>	0.01 - 0.67	0.19 (0.19)	0.01 - 0.79	0.23 (0.23)	0.01 - 0.63	0.14 (0.12)	0.02 - 0.62	0.21 (0.19)	0.01 - 0.88	0.29 (0.27)
Bulk canopy conductance*	cm s <sup>-1</sup>	0 - 9.7	2.1(1.8)	0 - 2.3	0.5(0.4)	0 - 8.9	2.1(1.9)	—	—	0 - 9.3	1.9(1.6)
CO <sub>2</sub> flux	μmol m <sup>-2</sup> s <sup>-1</sup>	-43.4 - 13.0	-7.7(-1.7)	-12.5 - 9.4	-0.7(0.7)	-45.3 - 10.9	-6.2(-1.1)	-5.7 - 2.8	-0.4(-0.1)	-40.3 - 11.1	-5.3(0.1)
Latent heat flux	W m <sup>-2</sup>	-211.6 - 551.4	119.5 (36.1)	-41.4 - 167.3	31.0 (17.2)	-225.8 - 385.7	62.3 (18.5)	-179.6 - 268.2	6.1(4.3)	-180.7 - 363.5	66.2 (36.1)
Sensible heat flux	W m <sup>-2</sup>	-139.8 - 144.1	-4.4(-3.8)	-93.1 - 343.6	59.3(2.7)	-111.8 - 216.7	13.3(-0.4)	-116.1 - 178.3	1.7(-0.2)	-243.9 - 167.6	11.6 (-2.9)
Ambient air Hg <sup>0</sup> conc.	ng m <sup>-3</sup>	2.22 - 12.57	5.19 (4.94)	1.77 - 10.09	3.90 (3.59)	1.87 - 10.57	3.42 (3.31)	2.71 - 13.02	6.22 (6.24)	1.21 - 7.28	3.72 (3.39)
Above-canopy Hg <sup>0</sup> flux	ng m <sup>-2</sup> h <sup>-1</sup>	-888.7 - 927.8	26.7 (13.4)	-491.8 - 467.6	16.5 (10.8)	-794.5 - 420.1	-11.8(-6.1)	-1051.5 - 508.9	-11.6 (-6.7)	-926.6 - 483.5	17.3 (12.2)
Hg <sup>0</sup> deposition velocity	cm s <sup>-1</sup>	-2.06 - 1.82	-0.12 (-0.10)	-1.86 - 1.34	-0.04 (-0.02)	-1.19 - 1.50	0.10 (0.07)	-2.95 - 1.99	0.01 (0.04)	-2.03 - 1.88	-0.19 (-0.12)
Hg <sup>0</sup> flux data coverage	%	[—]	74.0	[—]	82.2	[—]	86.1	[—]	83.0	[—]	51.3
Data with developed turbulence‡	%	[—]	68.9	[—]	75.2	[—]	67.7	[—]	70.9	[—]	68.0
Hg <sup>0</sup> flux data < MDL	%	[—]	54	[—]	61	[—]	57	[—]	59	[—]	64
Hg <sup>0</sup> flux uncertainty	%	[—]	(32)	[—]	(28)	[—]	(36)	[—]	(35)	[—]	(29)

689 \*Data for daytime when global radiation > 100 W m<sup>-2</sup>. †Data cover only the initial part of the campaign. ‡ Flux  
 690 data associated with turbulence quality classes 0 and 1.



691 **Table 2.** Spearman's rank-order correlation coefficients between Hg<sup>0</sup> flux (REA-method), Hg<sup>0</sup> air  
 692 concentration and other measured parameters. Significance levels p < 0.01, p < 0.001 are indicated by red  
 693 and black bold-faced fonts respectively.

Variable	May 2-18, 2012		June 12 - 29, 2012		Aug. 29 - Sept. 17, 2012		Jan. 12 - 24, 2013		April 1 - 24, 2013	
	Ambient air Hg <sup>0</sup>	Hg <sup>0</sup> flux	Ambient air Hg <sup>0</sup>	Hg <sup>0</sup> flux	Ambient air Hg <sup>0</sup>	Hg <sup>0</sup> flux	Ambient air Hg <sup>0</sup>	Hg <sup>0</sup> flux	Ambient air Hg <sup>0</sup>	Hg <sup>0</sup> flux
Air temperature	<b>0.15</b>	<b>-0.10</b>	<b>-0.44</b>	0.04	<b>0.30</b>	<b>-0.14</b>	<b>0.29</b>	0.05	<b>0.39</b>	0.06
Soil temperature	-0.01	<b>-0.13</b>	<b>-0.42</b>	0.01	<b>0.14</b>	<b>-0.22</b>	<b>0.17</b>	0.03	<b>0.21</b>	<b>0.11</b>
Air humidity	<b>0.12</b>	<b>0.19</b>	<b>0.19</b>	-0.05	-0.01	<b>0.17</b>	-0.01	<b>-0.10</b>	-0.00	<b>-0.21</b>
Global radiation	<b>0.20</b>	<b>-0.20</b>	<b>-0.18</b>	0.07	<b>0.28</b>	<b>-0.29</b>	<b>0.38</b>	<b>-0.16</b>	0.04	<b>0.19</b>
Leaf wetness	0.07	<b>0.14</b>	<b>0.28</b>	0.01	<b>-0.10</b>	<b>0.18</b>	<b>-0.14</b>	0.05	<b>0.18</b>	<b>-0.23</b>
PAR photon flux	<b>0.21</b>	<b>-0.19</b>	<b>-0.19</b>	0.07	<b>0.25</b>	<b>-0.27</b>	<b>0.38</b>	<b>-0.17</b>	0.04	<b>0.19</b>
Soil water content	<b>0.24</b>	<b>-0.19</b>	-0.01	-0.07	<b>-0.08</b>	0.03	<b>0.21</b>	0.01	—	—
Wind speed	<b>0.28</b>	<b>0.14</b>	<b>-0.23</b>	<b>0.35</b>	<b>0.17</b>	<b>-0.26</b>	<b>0.09</b>	<b>0.25</b>	<b>-0.26</b>	<b>0.37</b>
Friction velocity	<b>0.37</b>	<b>0.08</b>	<b>-0.21</b>	<b>0.29</b>	<b>0.22</b>	<b>-0.28</b>	0.08	<b>0.26</b>	<b>-0.37</b>	<b>0.13</b>
Bulk canopy conductance	<b>0.28*</b>	0.08*	-0.12*	<b>0.23*</b>	<b>0.19*</b>	-0.14*	—	—	<b>-0.23*</b>	<b>-0.33*</b>
CO <sub>2</sub> flux	<b>-0.25</b>	<b>0.25</b>	-0.02	0.01	<b>-0.19</b>	<b>0.23</b>	<b>-0.23</b>	<b>0.17</b>	-0.09	<b>-0.12</b>
Latent heat flux	<b>0.21</b>	<b>-0.14</b>	<b>-0.28</b>	0.00	<b>0.21</b>	<b>-0.25</b>	<b>0.15</b>	0.07	<b>-0.14</b>	0.07
Sensible heat flux	<b>0.09</b>	<b>-0.24</b>	-0.08	<b>-0.10</b>	<b>0.28</b>	<b>-0.12</b>	<b>0.42</b>	<b>-0.29</b>	<b>0.19</b>	0.05
Ambient air Hg <sup>0</sup>	[—]	<b>-0.30</b>	[—]	-0.03	[—]	<b>-0.26</b>	[—]	<b>-0.35</b>	[—]	-0.07
Hg <sup>0</sup> flux	<b>-0.30</b>	[—]	-0.03	[—]	<b>-0.26</b>	[—]	<b>-0.35</b>	[—]	-0.07	[—]

694 \*Data for daytime when global radiation > 100 W m<sup>-2</sup>.

695 Figure captions

696 **Figure 1.** Seasonal variation in LAI ( $\text{m}^2 \text{m}^{-2}$ , yellow filled circles) and canopy height (green filled  
697 diamonds) for 2012 - 2013 (in part). The duration of the five flux sampling periods (with numbers  
698 given in consecutive order) is indicated by magenta shaded boxes. The grey box resembles the time  
699 duration of a field inter-comparison (IC) of chamber and micro-meteorological flux measurement  
700 techniques to quantify  $\text{Hg}^0$  flux (Zhu et al., 2015a).

701

702 **Figure 2.** Polar histograms of 20-minute averaged  $5^\circ$  per bin  $\text{Hg}^0$  concentrations ( $\text{ng m}^{-3}$ ) classified into  
703 four magnitude levels ( $\leq 3$ ,  $> 3 - 4$ ,  $> 4 - 6$  and  $\geq 6 \text{ ng m}^{-3}$ ). The letter assigned to each pollution rose  
704 refers to the campaign number in consecutive order (a = 1, b = 2 etc.).

705

706 **Figure 3.** Diurnal variation in above-canopy  $\text{Hg}^0$  flux (Left panels) and  $\text{Hg}^0$  concentrations during the  
707 five campaigns. Box horizontal border lines represent 25<sup>th</sup> and 75<sup>th</sup> percentiles from bottom to top, the  
708 whiskers include 10<sup>th</sup> and 90<sup>th</sup> percentiles, and the outliers (open circles) encompass 5<sup>th</sup> and 95<sup>th</sup>  
709 percentiles. The solid line in the box represents median.

710

711 **Figure 4.** Time series of the selected measurement data for the individual campaigns at YCES in  
712 consecutive order (a. – e.). Panels from the top downwards: Air and below canopy surface soil temperature  
713 ( $^\circ\text{C}$ , maroon and red solid lines respectively) and global radiation ( $\text{W m}^{-2}$ , yellow solid line); event  
714 precipitation (mm, black solid line), relative humidity (% , blue dotted line), canopy wetness (% , grey-blue  
715 solid line) and soil water content (%-volume of field capacity, blue dashed line); wind speed ( $\text{m s}^{-1}$ , olive  
716 solid line) and wind direction ( $^\circ$ , brown open circles); Smoothed  $\text{Hg}^0$  ( $\text{ng m}^{-2} \text{h}^{-1}$ , black solid line) and  $\text{CO}_2$   
717 flux ( $\mu\text{mol m}^{-2} \text{s}^{-1}$ , magenta solid line); ambient air  $\text{Hg}^0$  concentration ( $\text{ng m}^{-3}$ , grey filled circles) and  
718 cumulative  $\text{Hg}^0$  flux ( $\mu\text{g m}^{-2}$ , maroon filled circles). Dates refer to China Standard Time (major ticks indicate  
719 midnight).  $\text{Hg}^0$  flux data were smoothed by a 9-point moving average, where the shaded grey area represents  
720 its standard deviation. In Fig. 4b, the blue arrow associated with caption “Harvest” indicate the end of wheat  
721 harvest that started on June, 23.

722

723 **Figure 5.** Diurnal variation in air-soil  $\text{Hg}^0$  flux measured by a DFC underneath the developed canopies  
724 (Upper: Campaign 1, middle: 2, lower: 3): Note the divergent axis scale for the plot in the middle  
725 panel. Box horizontal border lines represent 25<sup>th</sup> and 75<sup>th</sup> percentiles from bottom to top, the whiskers  
726 include 10<sup>th</sup> and 90<sup>th</sup> percentiles, and the outliers (open circles) encompass 5<sup>th</sup> and 95<sup>th</sup> percentiles. The  
727 solid line in the box represents median.

728

729 **Figure 6.** Local polynomial-smoothed diurnal curves of above-canopy (blue line) and ground (maroon  
730 line)  $\text{Hg}^0$  flux during campaign 1 (upper panel) and 3 (lower panel). Lines and envelopes depict mean  
731 and 90% confidence intervals. Note the divergent y-axis scales for the plots.

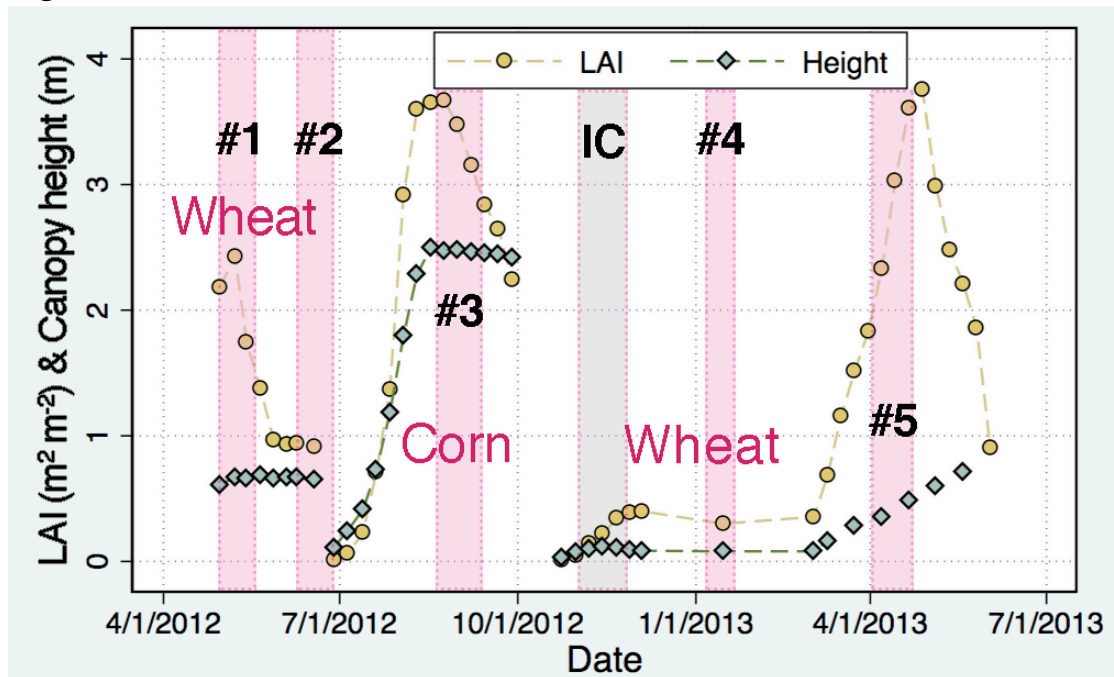
732

733 **Figure 7.** Time-series of latent heat flux ( $\text{W m}^{-2}$ , red filled squares),  $\text{Hg}^0$  flux (grey filled diamonds),  
734 wind direction ( $^\circ$ , yellow filled circles), soil water content (% of field capacity, dashed dark blue line)  
735 and leaf wetness (% , light blue solid line) measured during and after field irrigation (June, 26).

736

737 **Figure 8.** Time series (May 2012 – May 2013) of (a., upper panel) above-canopy (blue-shaded bars) and  
738 air-soil  $\text{Hg}^0$  flux (red-shaded bars) cumulated for each sampling campaign and (b., lower panel) of event  
739 measured (shaded bars, right axis) and THg wet deposition flux cumulated over the period (dotted blue  
740 line shaded down to abscissa, left axis).

741 Figures

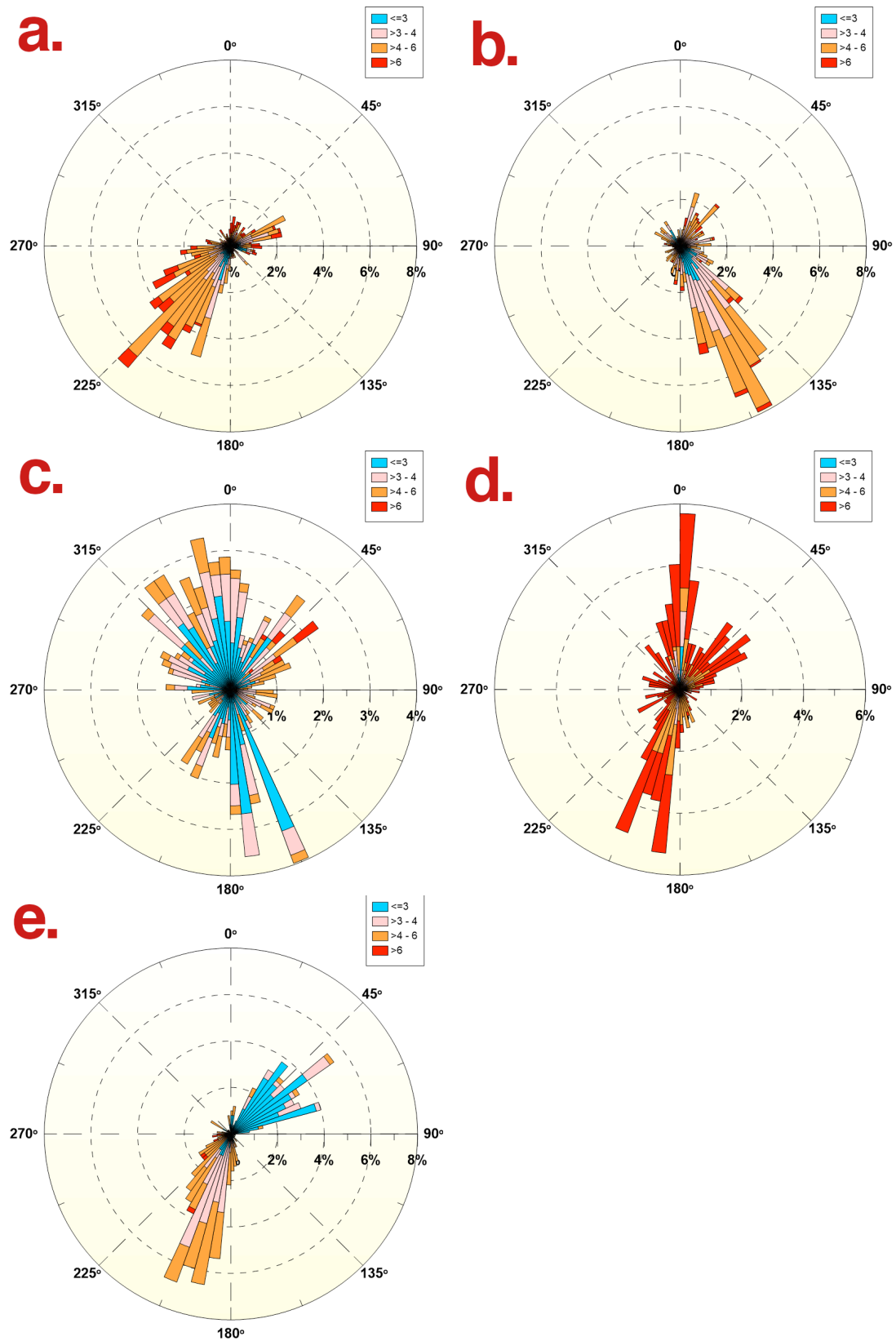


742

743 **Figure 1.** Seasonal variation in LAI (m<sup>2</sup> m<sup>-2</sup>, yellow filled circles) and canopy height (green filled  
744 diamonds) for 2012 - 2013 (in part). The duration of the five flux sampling periods (with numbers  
745 given in consecutive order) is indicated by magenta shaded boxes. The grey box resembles the time  
746 duration of a field inter-comparison (IC) of chamber and micro-meteorological flux measurement  
747 techniques to quantify Hg<sup>0</sup> flux (Zhu et al. 2015a).

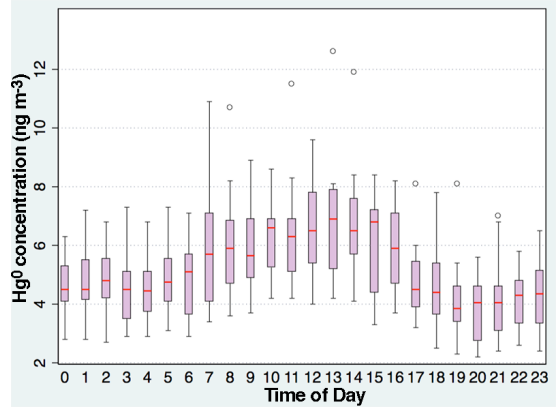
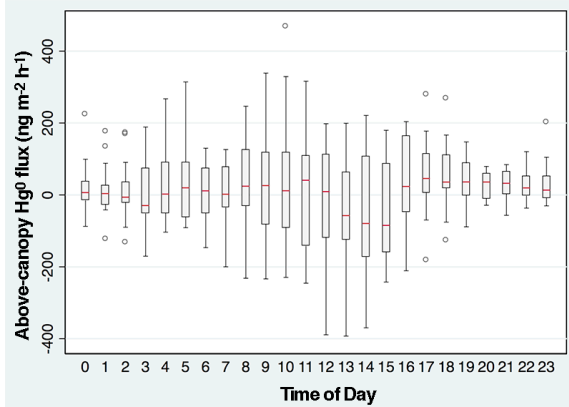
748

749

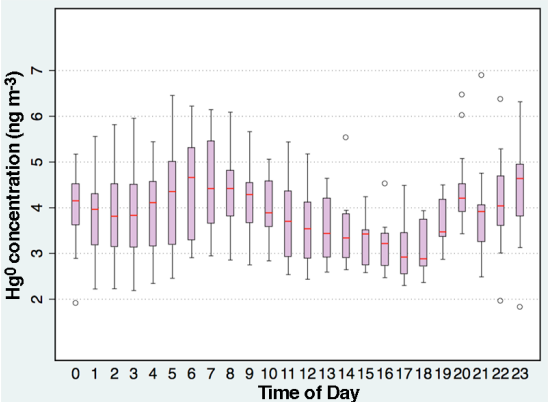
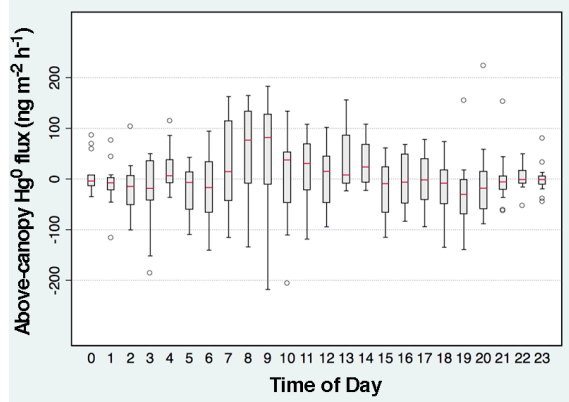


751 **Figure 2.** Polar histograms of 20-minute averaged 5° per bin  $Hg^0$  concentrations (ng  $m^{-3}$ ) classified into  
 752 four magnitude levels ( $\leq 3$ ,  $> 3 - 4$ ,  $> 4 - 6$  and  $\geq 6$  ng  $m^{-3}$ ). The letter assigned to each pollution rose  
 753 refers to the campaign number in consecutive order (a = 1, b = 2 etc.).

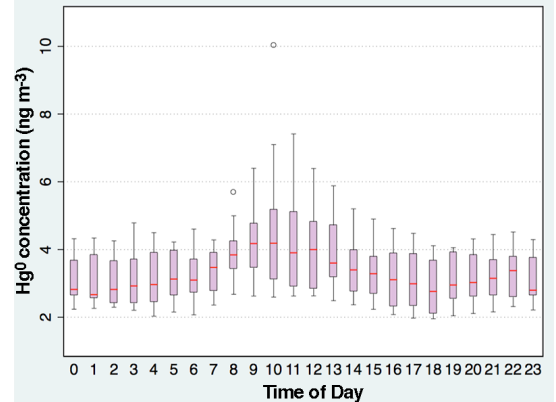
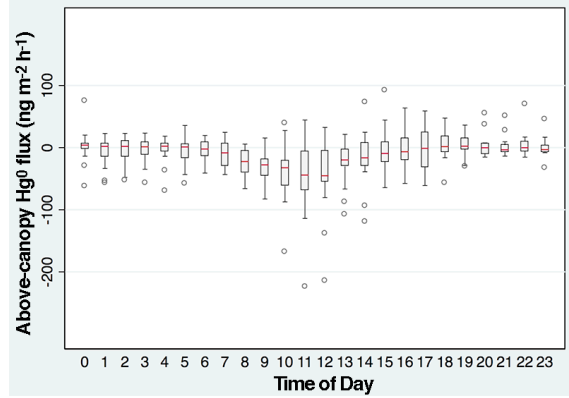
**Campaign 1, May 2 - 18, 2012 (Panel a, b)**



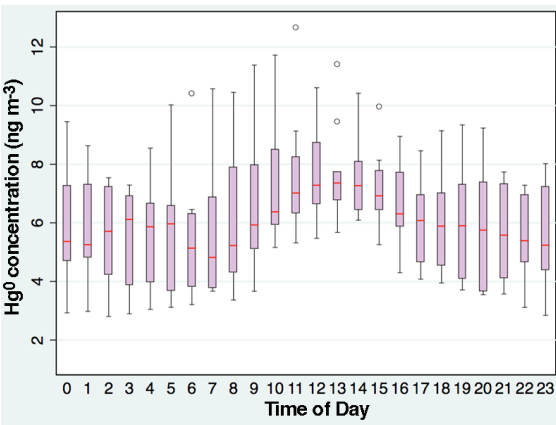
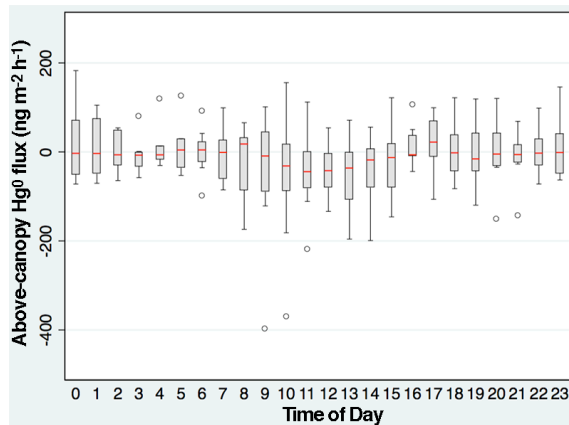
**Campaign 2, June 12 - 29, 2012 (Panel c, d)**



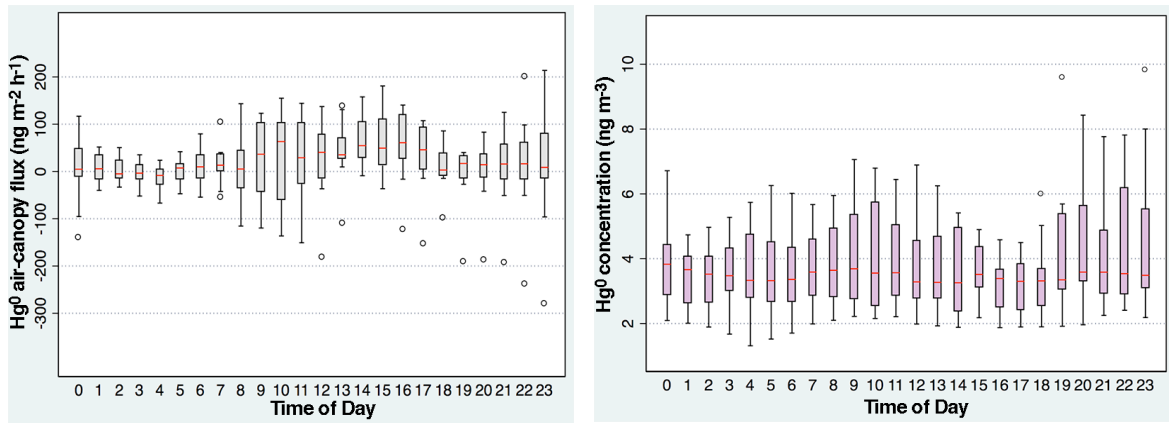
**Campaign 3, Aug. 29 - Sept. 17, 2012 (Panel e, f)**



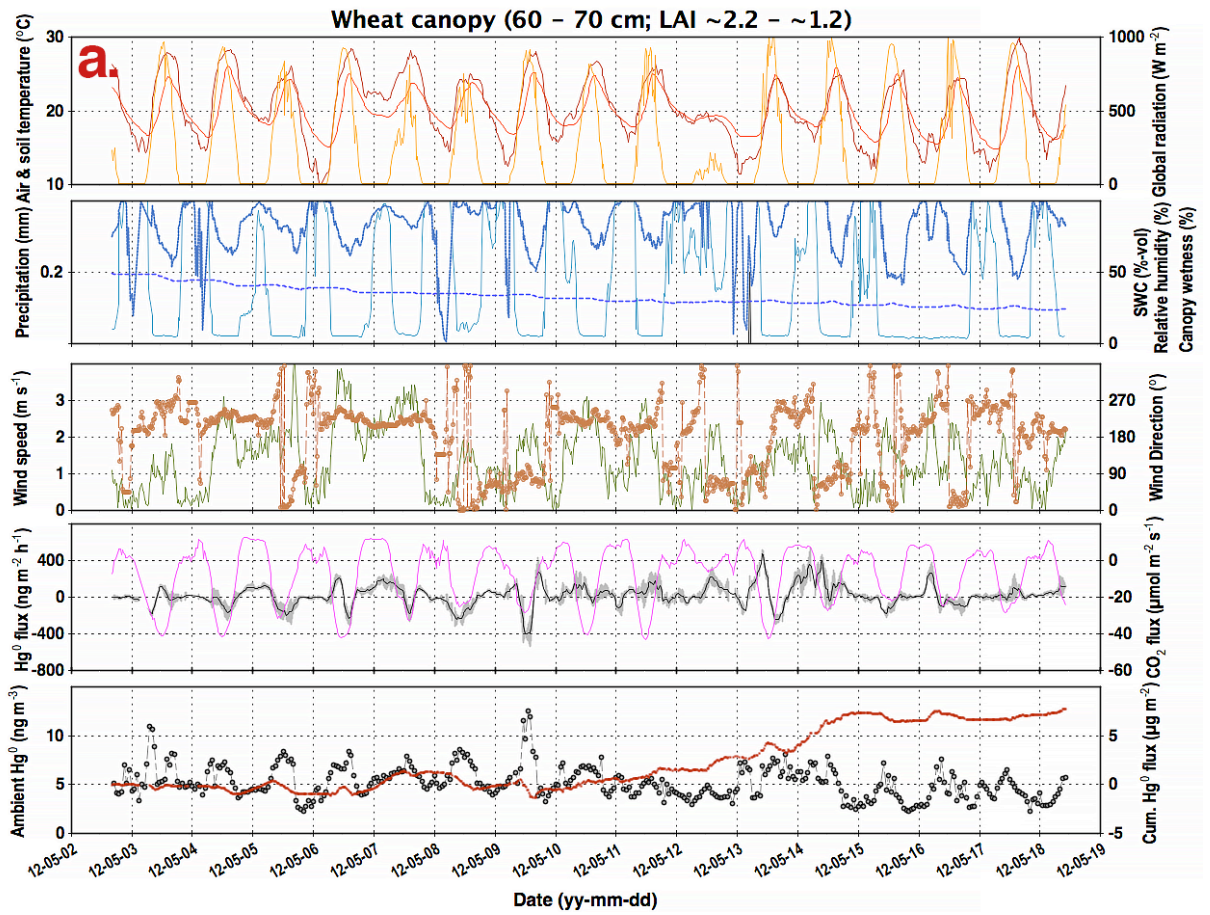
**Campaign 4, Jan. 12 - 24, 2013 (Panel g, h)**



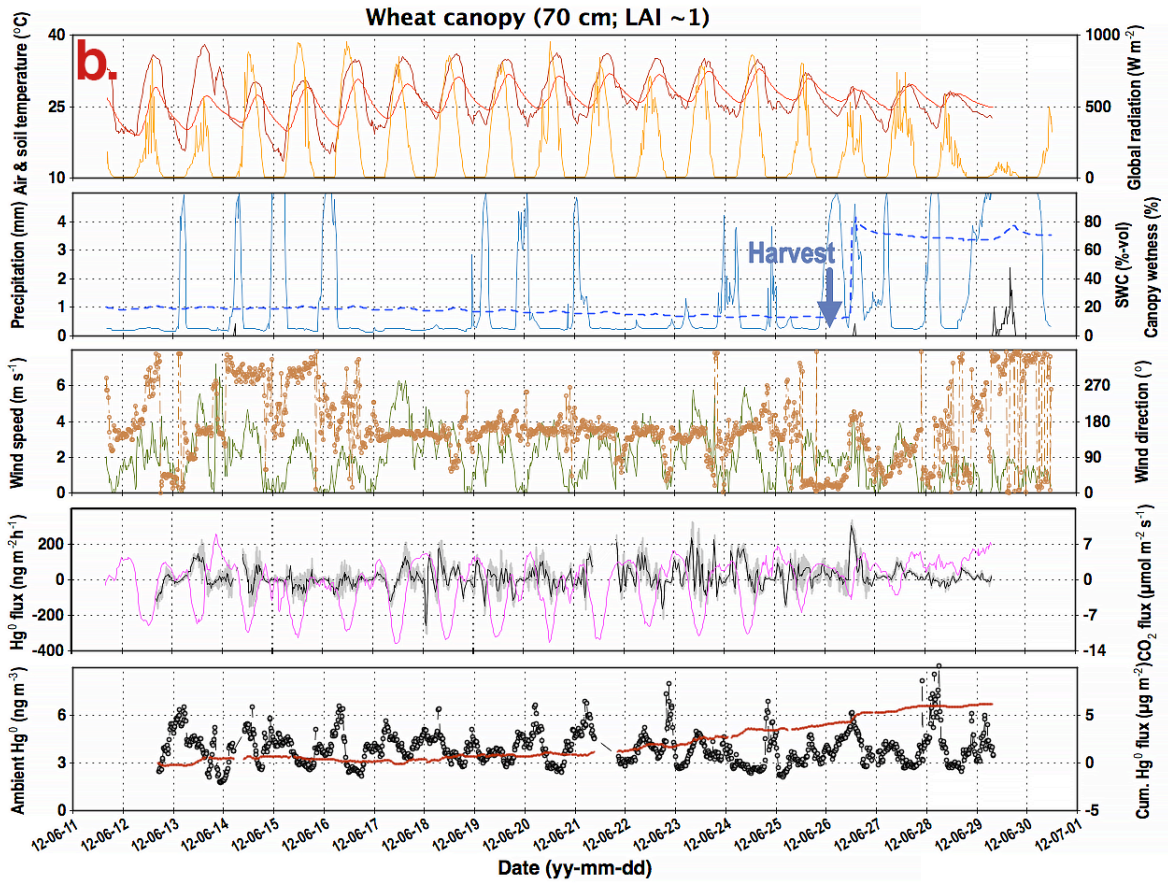
Campaign 5, April 1 - 24, 2013 (Panel I, j)

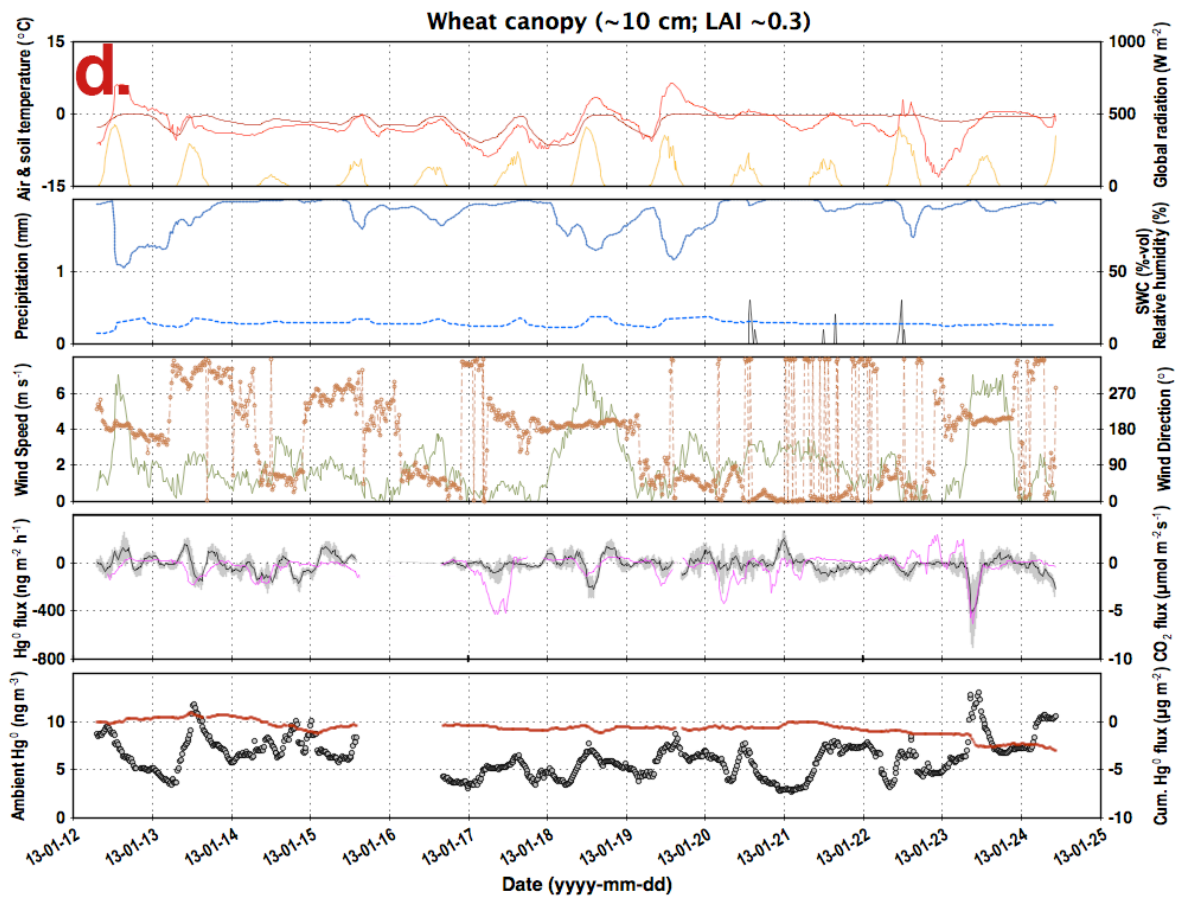
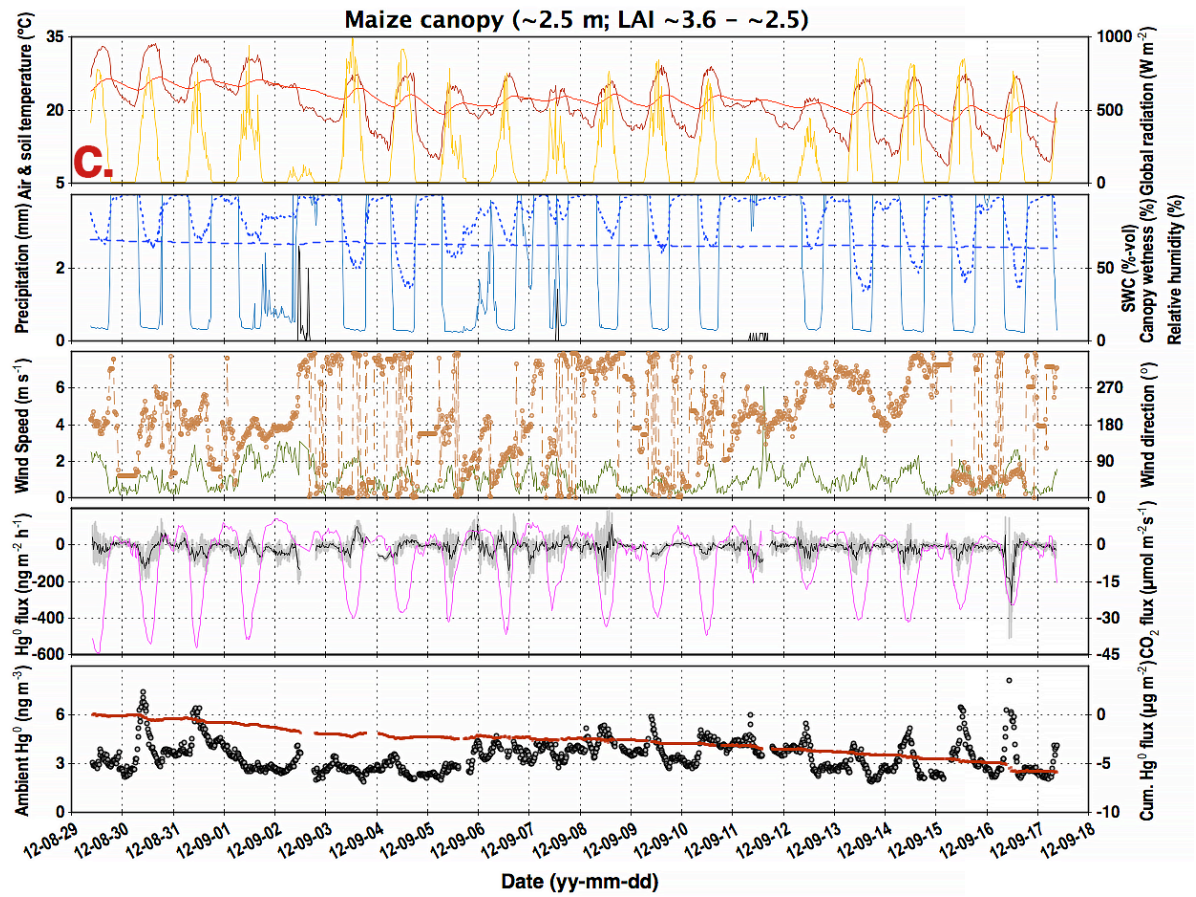


754 **Figure 3.** Diurnal variation in above-canopy Hg<sup>0</sup> flux (Left panels) and Hg<sup>0</sup> concentrations (Right  
755 panels) during the five campaigns.  
756

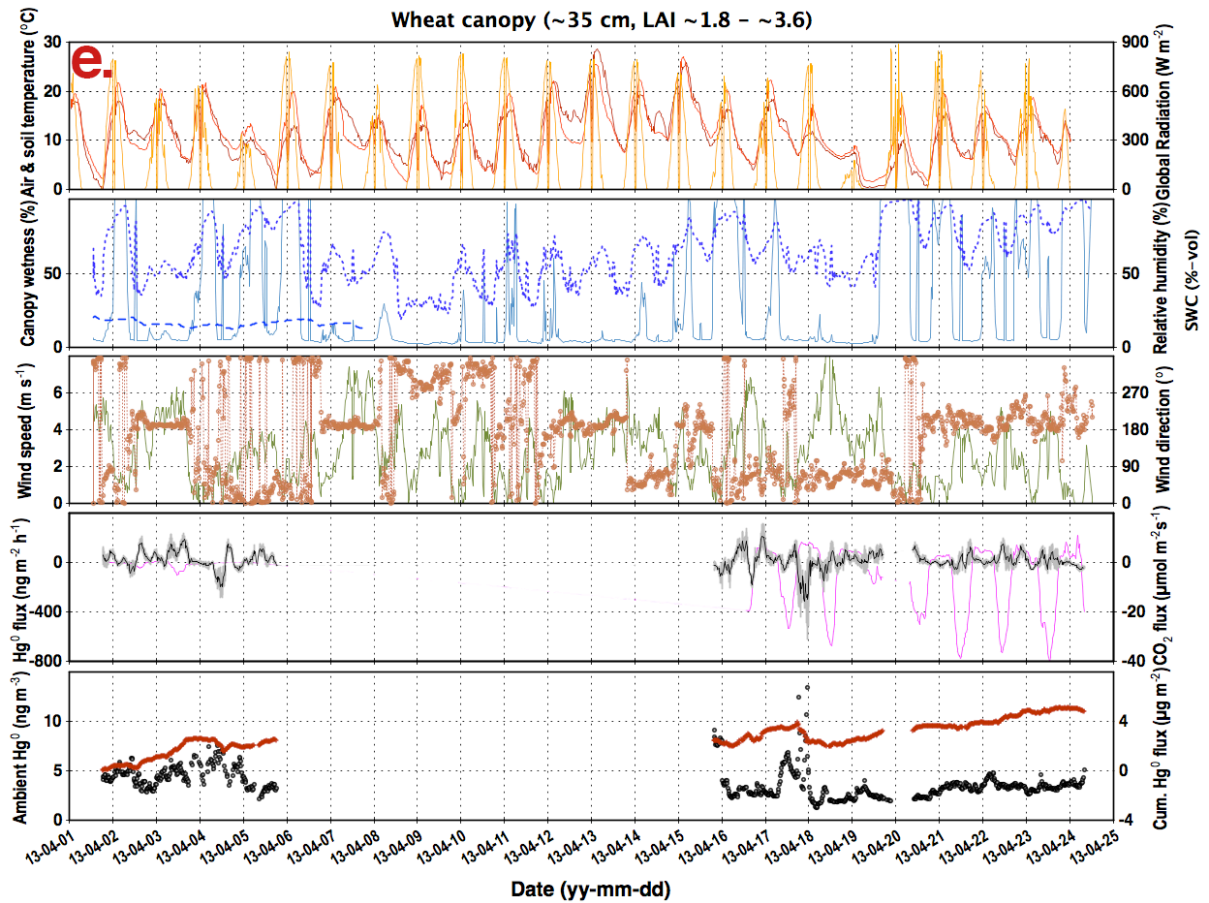


757



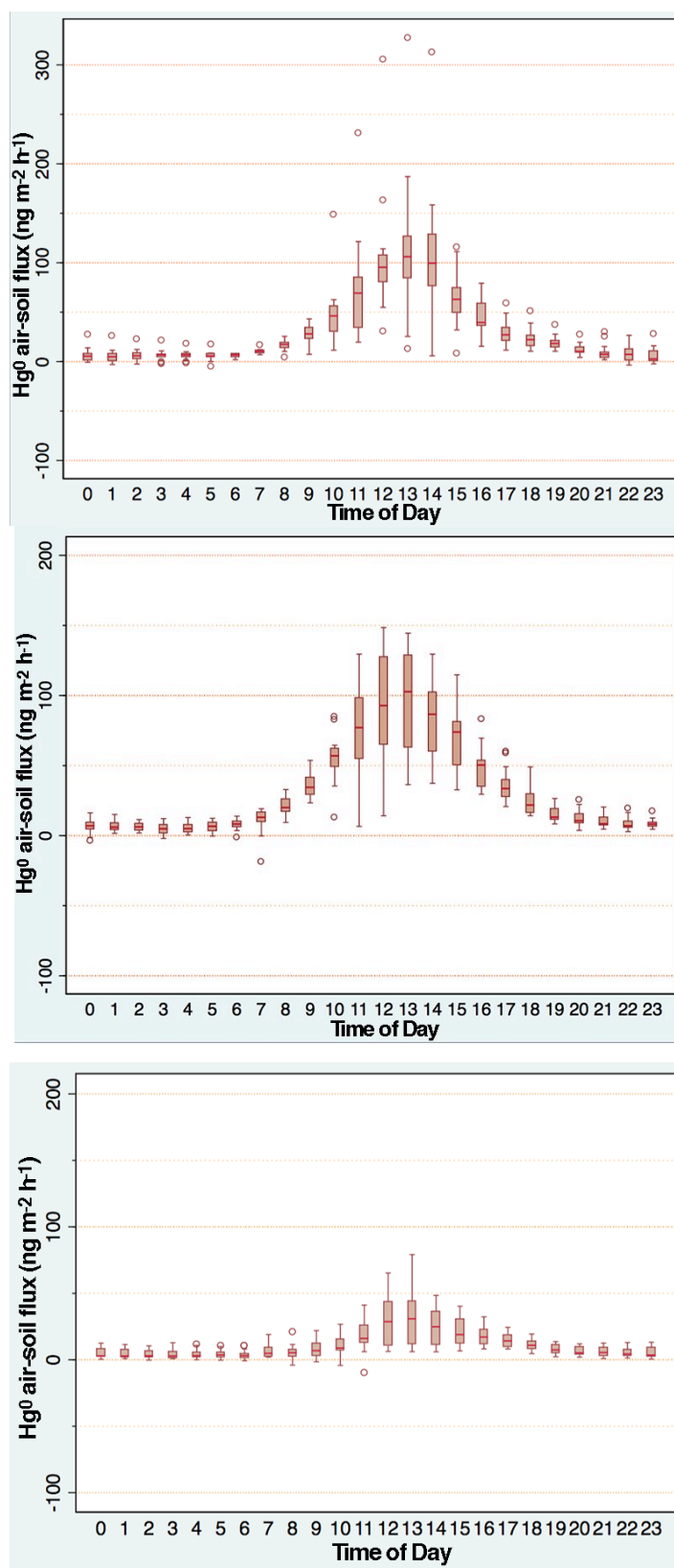




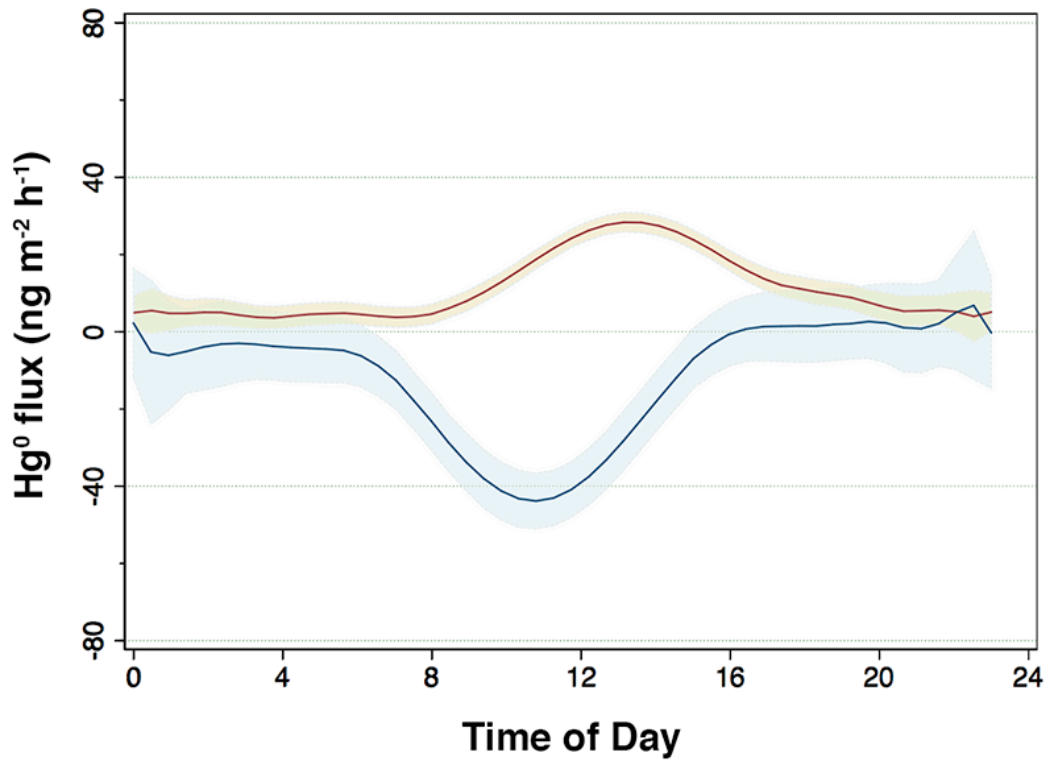
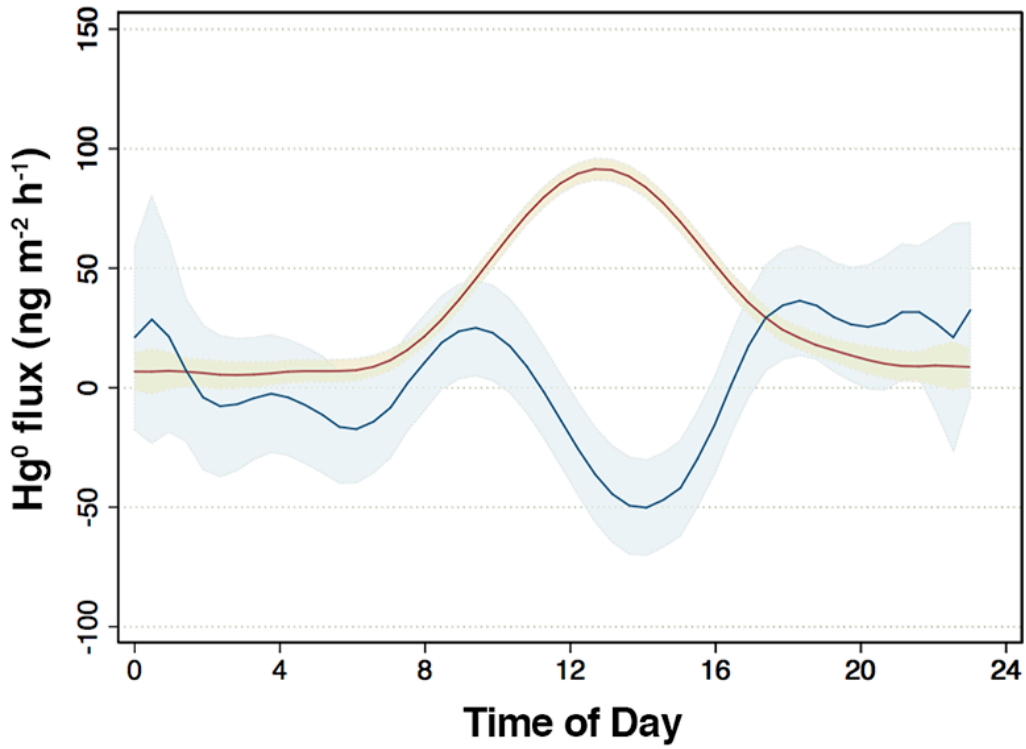


758  
 759  
 760  
 761  
 762  
 763  
 764  
 765  
 766  
 767  
 768  
 769  
 770

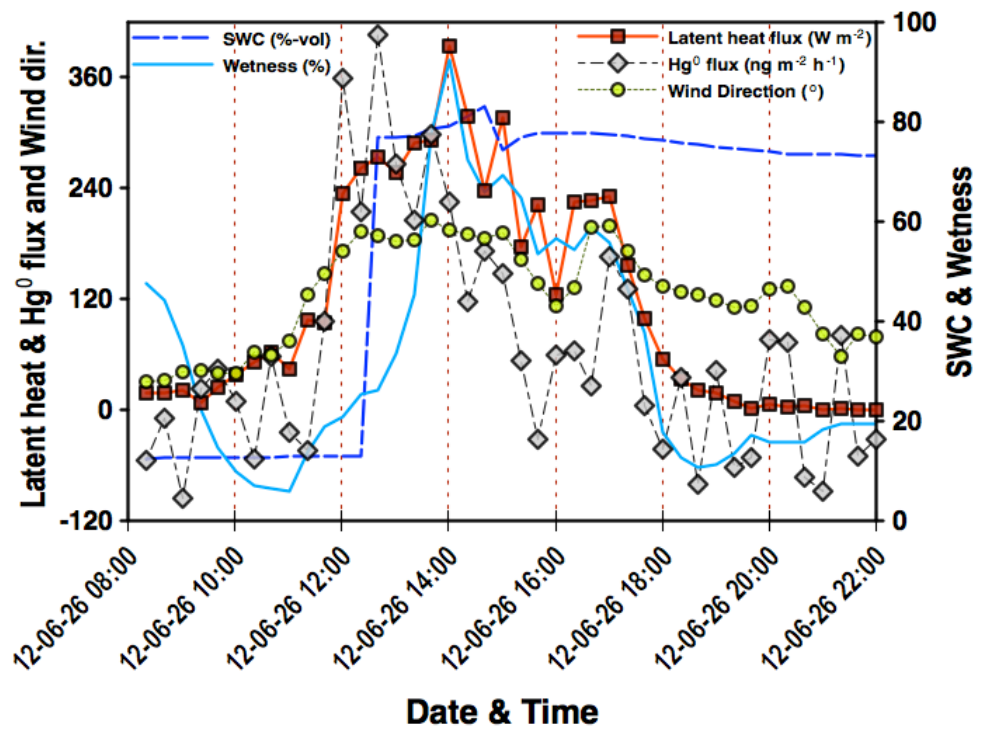
**Figure 4.** Time series of the selected measurement data for the individual campaigns at YCES in consecutive order (a. – e.). Panels from the top downwards: Air and below canopy surface soil temperature (°C, maroon and red solid lines respectively) and global radiation ( $\text{W m}^{-2}$ , yellow solid line); event precipitation (mm, black solid line), relative humidity (%), canopy wetness (%), soil water content (%-volume of field capacity, blue dashed line); wind speed ( $\text{m s}^{-1}$ , olive solid line) and wind direction ( $^{\circ}$ , brown open circles); Smoothed  $\text{Hg}^0$  ( $\text{ng m}^{-2} \text{h}^{-1}$ , black solid line) and  $\text{CO}_2$  flux ( $\mu\text{mol m}^{-2} \text{s}^{-1}$ , magenta solid line); ambient air  $\text{Hg}^0$  concentration ( $\text{ng m}^{-3}$ , grey filled circles) and cumulative  $\text{Hg}^0$  flux ( $\mu\text{g m}^{-2}$ , maroon filled circles). Dates refer to China Standard Time (major ticks indicate midnight).  $\text{Hg}^0$  flux data were smoothed by a 9-point moving average, where the shaded grey area represents its standard deviation. In Fig. 4b, the blue arrow associated with caption “Harvest” indicates the end of wheat harvest that started on June, 23.



772 **Figure 5.** Diurnal variation in air-soil  $\text{Hg}^0$  flux measured by a DFC underneath the developed canopies  
 773 (Upper: Campaign 1, middle: 2, lower: 3): Note the divergent axis scale for the plot in the upper panel.  
 774 Box horizontal border lines represent 25<sup>th</sup> and 75<sup>th</sup> percentiles from bottom to top, the whiskers include  
 775 10<sup>th</sup> and 90<sup>th</sup> percentiles. Open circles indicate outliers. The solid line in the box represents median.

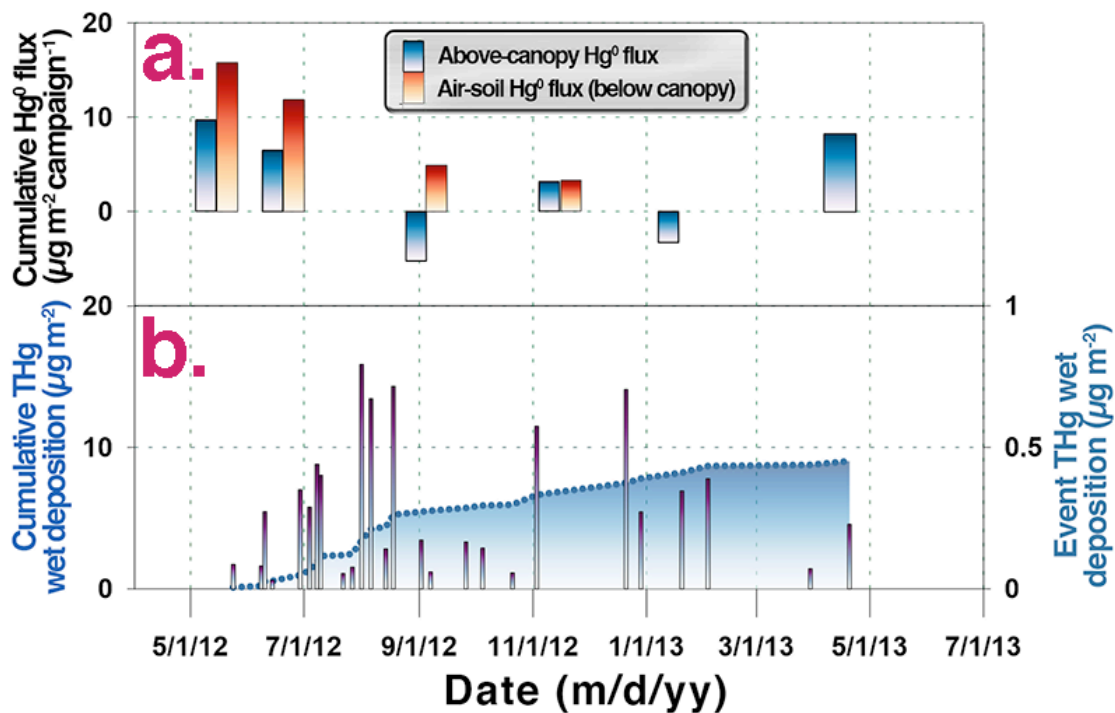


776 **Figure 6.** Local polynomial-smoothed diurnal curves of above-canopy (blue line) and ground  
 777 (maroon line)  $\text{Hg}^0$  flux during campaign 1 (upper panel) and 3 (lower panel). Lines and envelopes  
 778 depict mean and 90% confidence intervals. Note the divergent y-axis scales for the plots.  
 779  
 780



781  
 782  
 783  
 784  
 785  
 786

**Figure 7.** Time-series of latent heat flux ( $\text{W m}^{-2}$ , red filled squares),  $\text{Hg}^0$  flux ( $\text{ng m}^{-2} \text{h}^{-1}$ , grey filled diamonds), wind direction ( $^\circ$ , yellow filled circles), soil water content (%-vol. of field capacity, dashed dark blue line) and leaf wetness (% , light blue solid line) measured during and after field irrigation (June, 26).



788

789

790

791

792

**Figure 8.** Time series (May 2012 – May 2013) of (a., upper panel) above-canopy (blue-shaded bars) and air-soil Hg<sup>0</sup> flux (red-shaded bars) cumulated for each sampling campaign and (b., lower panel) of event measured (shaded bars, right axis) and THg wet deposition flux cumulated over the period (dotted blue line shaded down to abscissa, left axis).

793 **References**

794

795 AMAP/UNEP: Technical Background Report for the Global Mercury Assessment 2013, Arctic  
796 Monitoring and Assessment Programme, Oslo, Norway/UNEP Chemicals Branch, Geneva,  
797 Switzerland, vi + 263 pp., 2013.

798 Bahlmann, E., Ebinghaus, R., and Ruck, W.: Development and application of a laboratory flux  
799 measurement system (LFMS) for the investigation of the kinetics of mercury emissions from soils, J.  
800 Environ. Manage., 81, 114-125, 2006.

801 Bahlmann, E., Ebinghaus, R., and Ruck, W.: The effect of soil moisture on the emission of mercury  
802 from soils, Materials and Geoenvironment, 51, 791 - 794, 2004.

803 Bao, X. Y., Wen, X. F., Sun, X. M., Zhao, F. H., and Wang, Y. Y.: Interannual variation in carbon  
804 sequestration depends mainly on the carbon uptake period in two croplands on the North China Plain,  
805 PLoS ONE, 9, e110021, doi: 10.1371/journal.pone.0110021, 2014.

806 Bash, J. O. and Miller, D. R.: Growing season total gaseous mercury (TGM) flux measurements over  
807 an Acer rubrum L. stand, Atmos. Environ., 43, 5953-5961, 2009.

808 Bash, J. O. and Miller, D. R.: A note on elevated total gaseous mercury concentrations downwind from  
809 an agriculture field during tilling, Sci. Total Environ., 388, 379-388, 2007.

810 Battke, F., Ernst, D., and Halbach, S.: Ascorbate promotes emission of mercury vapour from plants,  
811 Plant Cell Environ., 28, 1487-1495, 2005.

812 Baya, A. P. and Van Heyst, B.: Assessing the trends and effects of environmental parameters on the  
813 behaviour of mercury in the lower atmosphere over cropped land over four seasons, Atmos. Chem. Phys.,  
814 10, 8617-8628, 2010.

815 Biester, H., Müller, G., and Schöler, H. F.: Binding and mobility of mercury in soils contaminated by  
816 emissions from chlor-alkali plants, Sci. Total Environ., 284, 191-203, 2002.

817 Briggs, C. and Gustin, M. S.: Building upon the Conceptual Model for Soil Mercury Flux: Evidence of  
818 a Link Between Moisture Evaporation and Hg Evasion, Water Air Soil Poll., 224, 2013.

819 Browne, C. L. and Fang, S. C.: Differential uptake of mercury vapor by gramineous C<sub>3</sub> and C<sub>4</sub> plants,  
820 Plant Physiol., 72, 1040-1042, 1983.

821 Browne, C. L. and Fang, S. C.: Uptake of mercury vapor by wheat - an assimilation model, Plant  
822 Physiol., 61, 430-433, 1978.

823 Burba, G.: Eddy covariance method for scientific, industrial, agricultural and regulatory applications: A  
824 field book on measuring ecosystem gas exchange and areal emission rates, LI-COR Biosciences,  
825 Lincoln, NE, USA, 331 pp., 2013.

826 Businger, J. A. and Oncley, S. P.: Flux measurement with conditional sampling, J. Atmos. Ocean. Techn.,  
827 7, 349-352, 1990.

828 Carpi, A. and Lindberg, S. E.: Sunlight-mediated emission of elemental mercury from soil amended  
829 with municipal sewage sludge, Environ. Sci. Technol., 31, 2085-2091, 1997.

830 Cavallini, A., Natali, L., Durante, M., and Maserti, B.: Mercury uptake, distribution and DNA affinity  
831 in durum wheat (Triticum durum Desf.) plants, Sci. Total Environ., 243, 119-127, 1999.

832 Cobbett, F. D. and Van Heyst, B. J.: Measurements of GEM fluxes and atmospheric mercury  
833 concentrations (GEM, RGM and Hg-p) from an agricultural field amended with biosolids in Southern  
834 Ont., Canada (October 2004-November 2004), Atmos. Environ., 41, 2270-2282, 2007.

835 Cobos, D. R., Baker, J. M., and Nater, E. A.: Conditional sampling for measuring mercury vapor  
836 fluxes, Atmos. Environ., 36, 4309-4321, 2002.

837 Converse, A. D., Riscassi, A. L., and Scanlon, T. M.: Seasonal variability in gaseous mercury fluxes  
838 measured in a high-elevation meadow, Atmos. Environ., 44, 2176-2185, 2010.

839 Cui L., Feng X., Lin C.-J., Wang X., Meng B., Wang X., Wang H.: Accumulation and translocation of  
840 <sup>198</sup>Hg in four crop species, Environ. Toxicol. Chem. 33, 334-340, 2014.

841 Dengel, S. and Grace, J.: Carbon dioxide exchange and canopy conductance of two coniferous forests  
842 under various sky conditions, Oecologia, 164, 797-808, 2010.

843 Driscoll, C. T., Mason, R. P., Chan, H. M., Jacob, D. J., and Pirrone, N.: Mercury as a global pollutant:  
844 Sources, pathways, and effects, *Environ. Sci. Technol.*, 47, 4967-4983, 2013.

845 Du, S. H. and Fang, S. C.: Catalase activity of C<sub>3</sub> and C<sub>4</sub> species and its relationship to mercury vapor  
846 uptake, *Environ. Exp. Bot.*, 23, 347-353, 1983.

847 Du, S. H. and Fang, S. C.: Uptake of elemental mercury vapor by C<sub>3</sub> species and C<sub>4</sub> species, *Environ.*  
848 *Exp. Bot.*, 22, 437-443, 1982.

849 Eckley, C. S., Parsons, M. T., Mintz, R., Lapalme, M., Mazur, M., Tordon, R., Elleman, R., Graydon,  
850 J. A., Blanchard, P., and St Louis, V.: Impact of closing Canada's largest point-source of mercury  
851 emissions on local atmospheric mercury concentrations, *Environ. Sci. Technol.*, 47, 10339-10348,  
852 2013.

853 Edwards, G. C. and Howard, D. A.: Air-surface exchange measurements of gaseous elemental mercury over  
854 naturally enriched and background terrestrial landscapes in Australia, *Atmos. Chem. Phys.*, 13, 5325-5336,  
855 2013.

856 Edwards, G. C., Rasmussen, P. E., Schroeder, W. H., Wallace, D. M., Halfpenny-Mitchell, L., Dias, G.  
857 M., Kemp, R. J., and Ausma, S.: Development and evaluation of a sampling system to determine  
858 gaseous Mercury fluxes using an aerodynamic micrometeorological gradient method, *J. Geophys. Res.*  
859 *-Atmos.*, 110, D10306, doi:10.1029/2004JD005187, 2005.

860 Engle, M. A., Gustin, M. S., Lindberg, S. E., Gertler, A. W., and Ariya, P. A.: The influence of ozone  
861 on atmospheric emissions of gaseous elemental mercury and reactive gaseous mercury from substrates,  
862 *Atmos. Environ.*, 39, 7506-7517, 2005.

863 Ericksen, J., Gustin, M., Lindberg, S. E., Olund, S. D., and Krabbenhoft, D.: Assessing the Potential for  
864 Re-emission of Mercury Deposited in Precipitation from Arid Soils Using a Stable Isotope, *Environ.*  
865 *Sci. Technol.*, 39, 8001-8007, 2005.

866 Ericksen, J. A. and Gustin, M. S.: Foliar exchange of mercury as a function of soil and air mercury  
867 concentrations, *Sci. Total Environ.*, 324, 271-279, 2004.

868 Ericksen, J. A., Gustin, M. S., Schorran, D. E., Johnson, D. W., Lindberg, S. E., and Coleman, J. S.:  
869 Accumulation of atmospheric mercury in forest foliage, *Atmos. Environ.*, 37, 1613-1622, 2003.

870 European Commission, 2002. Amended proposal for a Directive of the European Parliament and of the  
871 Council on undesirable substance and products in animal nutrition. Official Journal, 346e361. C 096 E,  
872 27/03/2001.

873 Fowler, D., Hargreaves, K. J., Skiba, U., Milne, R., Zahniser, M. S., Moncrieff, J. B., Beverland, I. J.,  
874 Gallagher, M. W., Ineson, P., Garland, J., and Johnson, C.: Measurements of CH<sub>4</sub> and N<sub>2</sub>O fluxes at the  
875 landscape scale using micrometeorological methods, *Phil. Trans. R. Soc. Lond. A*, 351, 339-356, 1995.

876 Fowler, D., Pilegaard, K., Sutton, M. A., Ambus, P., Raivonen, M., Duyzer, J., Simpson, D., Fagerli, H.,  
877 Fuzzi, S., Schjörring, J. K., Granier, C., Neftel, A., Isaksen, I. S. A., Laj, P., Maione, M., Monks, P. S.,  
878 Burkhardt, J., Daemmgen, U., Neiryneck, J., Personne, E., Wichink-Kruit, R., Butterbach-Bahl, K.,  
879 Flechard, C., Tuovinen, J. P., Coyle, M., Gerosa, G., Loubet, B., Altimir, N., Grünhage, L., Ammann, C.,  
880 Cieslik, S., Paoletti, E., Mikkelsen, T. N., Ro-Poulsen, H., Cellier, P., Cape, J. N., Horvath, L., Loreto, F.,  
881 Niinemets, U., Palmer, P. I., Rinne, J., Misztal, P., Nemitz, E., Nilsson, D., Pryor, S., Gallagher, M. W.,  
882 Vesala, T., Skiba, U., Brüggemann, N., Zechmeister-Boltenstern, S., Williams, J., O'Dowd, C., Facchini,  
883 M. C., de Leeuw, G., Flossman, A., Chaumerliac, N., and Erisman, J. W.: Atmospheric composition  
884 change: Ecosystems-Atmosphere interactions, *Atmos. Environ.*, 43, 5193-5267, 2009.

885 Frescholtz, T. F., Gustin, M. S., Schorran, D. E., and Fernandez, G. C. J.: Assessing the source of  
886 mercury in foliar tissue of quaking aspen, *Environ. Toxicol. Chem.*, 22, 2114-2119, 2003.

887 Fritsche, J., Obrist, D., and Alewell, C.: Evidence of microbial control of Hg<sup>0</sup> emissions from  
888 uncontaminated terrestrial soils, *J. Plant Nutr. Soil Sci.*, 171, 200-209, 2008a.

889 Fritsche, J., Obrist, D., Zeeman, M. J., Conen, F., Eugster, W., and Alewell, C.: Elemental mercury  
890 fluxes over a sub-alpine grassland determined with two micrometeorological methods, *Atmos.*  
891 *Environ.*, 42, 2922-2933, 2008b.

892 Fritsche, J., Wohlfahrt, G., Ammann, C., Zeeman, M., Hammerle, A., Obrist, D., and Alewell, C.:  
893 Summertime elemental mercury exchange of temperate grasslands on an ecosystem-scale, *Atmos.*  
894 *Chem. Phys.*, 8, 7709-7722, 2008c.

895 Fu, X., Feng, X., Zhang, H., Yu, B., and Chen, L.: Mercury emissions from natural surfaces highly  
896 impacted by human activities in Guangzhou province, South China, *Atmos. Environ.*, 54, 185-193, 2012.

897 Fu, X. W., Feng, X. B., and Wang, S. F.: Exchange fluxes of Hg between surfaces and atmosphere in  
898 the eastern flank of Mount Gongga, Sichuan province, southwestern China, *J. Geophys. Res. –Atmos.*,  
899 113, D20306, doi: 10.1029/2008jd009814, 2008.

900 Fu, X. W., Zhang, H., Wang, X., Yu, B., Lin, C. J., and Feng, X. B.: Observations of atmospheric  
901 mercury in China: a critical review, *Atmos. Chem. Phys. Discuss.*, 15, 11925-11983, doi:10.5194/acpd-15-  
902 11925-2015 ,2015.

903 Gillis, A. A. and Miller, D. R.: Some local environmental effects on mercury emission and absorption  
904 at a soil surface, *Sci. Total Environ.*, 260, 191-200, 2000.

905 Graydon, J. A., St Louis, V. L., Lindberg, S. E., Hintelmann, H., and Krabbenhoft, D. P.: Investigation  
906 of mercury exchange between forest canopy vegetation and the atmosphere using a new dynamic  
907 chamber, *Environ. Sci. Technol.*, 40, 4680-4688, 2006.

908 Graydon, J. A., St Louis, V. L., Lindberg, S. E., Sandilands, K. A., Rudd, J. W. M., Kelly, C. A., Harris, R.,  
909 Tate, M. T., Krabbenhoft, D. P., Emmerton, C. A., Asmath, H., and Richardson, M.: The role of terrestrial  
910 vegetation in atmospheric Hg deposition: Pools and fluxes of spike and ambient Hg from the METAALICUS  
911 experiment, *Global Biogeochemical Cycles*, 26, GB1022, doi:10.1029/2011GB004031, 2012.

912 Grigal, D. F.: Mercury sequestration in forests and peatlands: A review, *J. Environ. Qual.*, 32, 393-405,  
913 2003.

914 Grossman-Clarke, S., Kimball, B. A., Hunsaker, D. J., Long, S. P., Garcia, R. L., Kartschall, T., Wall,  
915 G. W., Printer, P. J., Wechsung, F., and LaMorte, R. L.: Effects of elevated atmospheric CO<sub>2</sub> on  
916 canopy transpiration in senescent spring wheat, *Agric. For. Meteorol.*, 93, 95-109, 1999.

917 Gustin, M. S.: Exchange of mercury between the atmosphere and terrestrial ecosystems. In: *Advances  
918 in Environmental Chemistry and Toxicology of Mercury*, Cai, Y., Liu, G., and O'Driscoll, N. J. (Eds.),  
919 John Wiley & Sons, 423–451, 2011.

920 Gustin, M. S., Taylor, G. E., and Maxey, R. A.: Effect of temperature and air movement on the flux of  
921 elemental mercury from substrate to the atmosphere, *J. Geophys. Res. –Atmos.*, 102, 3891-3898, 1997.

922 Hall, C., Mao, H., Ye, Z., Talbot, R., Ding, A., Zhang, Y., Zhu, J., Wang, T., Lin, C.-J., Fu, C., and  
923 Yang, X.: Sources and dynamic processes controlling background and peak concentrations of TGM in  
924 Nanjing, China, *Atmosphere*, 5, 124-155, 2014.

925 Hanson, P. J., Lindberg, S. E., Tabberer, T. A., Owens, J. G., and Kim, K. H.: Foliar Exchange of  
926 Mercury-Vapor - Evidence for a Compensation Point, *Water Air Soil Poll.*, 80, 373-382, 1995.

927 Hintelmann, H., Harris, R., Heyes, A., Hurley, J. P., Kelly, C. A., Krabbenhoft, D. P., Lindberg, S.,  
928 Rudd, J. W. M., Scott, K. J., and St Louis, V. L.: Reactivity and mobility of new and old mercury  
929 deposition in a Boreal forest ecosystem during the first year of the METAALICUS study, *Environ. Sci.  
930 Technol.*, 36, 5034-5040, 2002.

931 Huang, X., Li, M., Friedli, H. R., Song, Y., Chang, D., and Zhu, L.: Mercury emissions from biomass  
932 burning in China, *Environ. Sci. Technol.*, 45, 9442-9448, 2011.

933 Kaimal, J. C., Wyngaard, J. C., Izumi, Y., and Coté, O. R.: Spectral characteristics of surface layer  
934 turbulence, *Q. J. Roy. Meteor. Soc.*, 98, 563-589, 1972.

935 Keeler, G. J., Landis, M. S., Norris, G. A., Christianson, E. M., and Dvonch, J. T.: Sources of mercury  
936 wet deposition in Eastern Ohio, USA, *Environ. Sci. Technol.*, 40, 5874-5881, 2006.

937 Khozhina E.I., Paleskii S.V., Saprykin A.I. Migration of heavy metals to the atmosphere in the process  
938 of transpiration, *Atmos. Ocean. Optics*, 14, 553 - 556, 2001 (In Russian with English summary).

939 Kim, K. H., Lindberg, S. E., and Meyers, T. P.: Micrometeorological measurements of mercury vapor  
940 fluxes over background forest soils in eastern Tennessee, *Atmos. Environ.*, 29, 267-282, 1995.

941 Kramm, G., Beier, N., Dlugi, R., and Müller, H.: Evaluation of conditional sampling methods, *Beitr.  
942 Phys. Atmos.*, 72, 161-172, 1999.

943 Landa, E. R.: Soil-water content and temperature as factors in volatile loss of applied mercury(II) from  
944 soils, *Soil Sci.*, 126, 44-48, 1978.



- 945 Lee, X.: Water vapor density effect on measurements of trace gas mixing ratio and flux with a  
946 massflow controller, *J. Geophys. Res. –Atmos.*, 105, 17807-17810, 2000.
- 947 Lee, X., Benoit, G., and Hu, X.: Total gaseous mercury concentration and flux over a coastal saltmarsh  
948 vegetation in Connecticut, USA, *Atmos. Environ.*, 34, 4205-4213, 2000.
- 949 Li, J., Yu, Q., Sun, X. M., Tong, X. J., Ren, C. Y., Wang, J., Liu, E. M., Zhu, Z. L., and Yu, G. R.:  
950 Carbon dioxide exchange and the mechanism of environmental control in a farmland ecosystem in  
951 North China Plain, *Sci. China Ser. D*, 49, 226-240, 2006.
- 952 Li, L., Nielsen, D. C., Yu, Q., Ma, L., and Ahuja, L. R.: Evaluating the crop water stress index and its  
953 correlation with latent heat and CO<sub>2</sub> fluxes over winter wheat and maize in the North China Plain,  
954 *Agric. Wat. Manage.*, 97, 1146-1155, 2010.
- 955 Lin, C.-J., Zhu, W., Li, X., Feng, X., Sommar, J., and Shang, L.: Novel dynamic flux chamber for  
956 measuring air-surface exchange of Hg<sup>0</sup> from soils, *Environ. Sci. Technol.*, 46, 8910-8920, 2012.
- 957 Lin, J., Wang, W. Y., Li, Y. H., and Yang, L. S.: Heavy metals in soil and crops of an intensively  
958 farmed area: A case study in Yucheng City, Shandong province, China, *Int. J. Environ. Res. Public  
959 Health*, 7, 395-412, 2010.
- 960 Lindberg, S. E., Meyers, T. P., Taylor, G. E., Turner, R. R., and Schroeder, W. H.: Atmosphere-surface  
961 exchange of mercury in a forest - Results of modeling and gradient approaches, *J. Geophys. Res. –  
962 Atmos.*, 97, 2519-2528, 1992.
- 963 Lindberg, S. E., Zhang, H., Gustin, M., Vette, A., Marsik, F., Owens, J., Casimir, A., Ebinghaus, R.,  
964 Edwards, G., Fitzgerald, C., Kemp, J., Kock, H. H., London, J., Majewski, M., Poissant, L., Pilote, M.,  
965 Rasmussen, P., Schaedlich, F., Schneeberger, D., Sommar, J., Turner, R., Wallschläger, D., and Xiao,  
966 Z.: Increases in mercury emissions from desert soils in response to rainfall and irrigation, *J. Geophys.  
967 Res. –Atmos.*, 104, 21879-21888, 1999.
- 968 Marsik, F. J., Keeler, G. J., Lindberg, S. E., and Zhang, H.: Air-surface exchange of gaseous mercury over a  
969 mixed Sawgrass-Cattail stand within the Florida Everglades, *Environ. Sci. Technol.*, 39, 4739-4746, 2005.
- 970 Mauclair, C., Layshock, J., and Carpi, A.: Quantifying the effect of humic matter on the emission of  
971 mercury from artificial soil surfaces, *Appl. Geochem.*, 23, 594-601, 2008.
- 972 Mauder, M. and Foken, T.: Documentation and instruction manual of EC Software Package TK2,  
973 Department of Micrometeorology, University of Bayreuth, *Arbeitsergebnisse* 26, 45 pp., 2004.
- 974 Meng, B., Feng, X., Qiu, G., Cai, Y., Wang, D., Li, P., Shang, L., and Sommar, J.: Distribution patterns  
975 of inorganic mercury and methylmercury in tissues of Rice (*Oryza sativa* L.) plants and possible  
976 bioaccumulation pathways, *J. Agric. Food Chem.*, 58, 4951-4958, 2010.
- 977 Millhollen, A. G., Obrist, D., and Gustin, M. S.: Mercury accumulation in grass and forb species as a  
978 function of atmospheric carbon dioxide concentrations and mercury exposures in air and soil,  
979 *Chemosphere*, 65, 889-897, 2006.
- 980 Moncrieff, J. B., Beverland, I. J., Ónéill, D. H., and Cropley, F. D.: Controls on trace gas exchange  
981 observed by a conditional sampling method, *Atmos. Environ.*, 32, 3265-3274, 1998.
- 982 NBSC: China Statistical Yearbook, National Bureau of Statistics of China, Beijing, China, 1998.
- 983 Nemitz, E., Flynn, M., Williams, P. I., Milford, C., Theobald, M. R., Blatter, A., Gallagher, M. W., and  
984 Sutton, M. A.: A relaxed eddy accumulation system for the automated measurement of atmospheric  
985 ammonia fluxes, *Water Air Soil Poll. Focus*, 1, 189-202, 2001.
- 986 Niu, Z. C., Zhang, X. S., Wang, S., Zeng, M., Wang, Z. W., Zhang, Y., and Ci, Z. J.: Field controlled  
987 experiments on the physiological responses of maize (*Zea mays* L.) leaves to low-level air and soil  
988 mercury exposures, *Environ. Sci. Poll. Res.*, 21, 1541-1547, 2014.
- 989 Niu, Z. C., Zhang, X. S., Wang, Z. W., and Ci, Z. J.: Field controlled experiments of mercury  
990 accumulation in crops from air and soil, *Environ. Poll.*, 159, 2684-2689, 2011.
- 991 Obrist, D.: Atmospheric mercury pollution due to losses of terrestrial carbon pools?, *Biogeochemistry*,  
992 85, 119-123, 2007.
- 993 Poissant, L., Pilote, M., Constant, P., Beauvais, C., Zhang, H. H., and Xu, X. H.: Mercury gas  
994 exchanges over selected bare soil and flooded sites in the bay St. Francois wetlands (Quebec, Canada),  
995 *Atmos. Environ.*, 38, 4205-4214, 2004.

- 996 Poissant, L., Pilote, M., Yumvihoze, E., and Lean, D.: Mercury concentrations and foliage/atmosphere  
997 fluxes in a maple forest ecosystem in Québec, Canada, *J. Geophys. Res. –Atmos.*, 113, D10307,  
998 doi:10.1029/2007JD009510, 2008.
- 999 Rinklebe, J., During, A., Overesch, M., Du Laing, G., Wennrich, R., Stärk, H. J., and Mothes, S.:  
1000 Dynamics of mercury fluxes and their controlling factors in large Hg-polluted floodplain areas,  
1001 *Environ. Pollut.*, 158, 308-318, 2010.
- 1002 Schlüter, K.: Review: Evaporation of mercury from soils. An integration and synthesis of current  
1003 knowledge, *Environ. Geol.*, 39, 249-271, 2000.
- 1004 Schroeder, W. H., Beauchamp, S., Edwards, G., Poissant, L., Rasmussen, P., Tordon, R., Dias, G.,  
1005 Kemp, J., Van Heyst, B., and Banic, C. M.: Gaseous mercury emissions from natural sources in  
1006 Canadian landscapes, *J. Geophys. Res. –Atmos.*, 110, D18302, doi:10.1029/2004JD005699, 2005.
- 1007 Schwesig, D. and Matzner, E.: Pools and fluxes of mercury and methylmercury in two forested  
1008 catchments in Germany, *Sci. Total Environ.*, 260, 213-223, 2000.
- 1009 Selin, N. E.: Global biogeochemical cycling of mercury: A review, *Annu. Rev. Environ. Resour.*, 34, 43–63, 2009.
- 1010 Sigler, J. M. and Lee, X.: Gaseous mercury in background forest soil in the northeastern United States.  
1011 *J. Geophys. Res. –Biogeo.*, 111, G02007, doi:10.1029/2005jg000106, 2006.
- 1012 Smith, L. M. and Reinfelder, J. R.: Mercury volatilization from salt marsh sediments, *J. Geophys. Res.*  
1013 *–Biogeo.*, 114, G00C09, doi:10.1029/2009jg000979, 2009.
- 1014 Smith-Downey, N. V., Sunderland, E. M., and Jacob, D. J.: Anthropogenic impacts on global storage  
1015 and emissions of mercury from terrestrial soils: Insights from a new global model, *J. Geophys. Res. –*  
1016 *Biogeo.*, 115, G03008, doi: 10.1029/2009jg001124, 2010.
- 1017 Sommar, J., Zhu, W., Lin, C. -J., and Feng, X.: Field approaches to measure Hg exchange between  
1018 natural surfaces and the atmosphere - A review, *Crit. Rev. Env. Sci Technol.*, 43, 1657-1739, 2013a.
- 1019 Sommar, J., Zhu, W., Shang, L. H., Feng, X. B., and Lin, C. -J.: A whole-air relaxed eddy  
1020 accumulation measurement system for sampling vertical vapour exchange of elemental mercury,  
1021 *Tellus B*, 65, doi: 10.3402/tellusb.v65i0.19940, 2013b.
- 1022 Song, X. and Van Heyst, B.: Volatilization of mercury from soils in response to simulated  
1023 precipitation, *Atmos. Environ.*, 39, 7494 - 7505, 2005.
- 1024 Song, S., Selin, N. E., Sørensen, A. L., Angot, H., Artz, R., Brooks, S., Brunke, E. G., Conley, G.,  
1025 Dommergue, A., Ebinghaus, R., Holsen, T. M., Jaffe, D. A., Kang, S., Kelley, P., Luke, W. T., Magand, O.,  
1026 Marumoto, K., Pfaffhuber, K. A., Ren, X., Sheu, G. R., Slemr, F., Warneke, T., Weigelt, A., Weiss-Penzias,  
1027 P., Wip, D. C., and Zhang, Q.: Top-down constraints on atmospheric mercury emissions and  
1028 implications for global biogeochemical cycling, *Atmos. Chem. Phys. Discuss.*, 15, 5269-5325, 2015.
- 1029 St Louis, V. L., Rudd, J. W. M., Kelly, C. A., Hall, B. D., Rolffhus, K. R., Scott, K. J., Lindberg, S. E.,  
1030 and Dong, W.: Importance of the forest canopy to fluxes of methyl mercury and total mercury to boreal  
1031 ecosystems, *Environ. Sci. Technol.*, 35, 3089-3098, 2001.
- 1032 Streets, D. G., Hao, J., Wu, Y., Jiang, J., Chan, M., Tian, H., and Feng, X.: Anthropogenic mercury  
1033 emissions in China, *Atmos. Environ.*, 39, 7789-7806, 2005.
- 1034 Thom, A. S.: Momentum, mass and heat exchange in plant communities. In: *Vegetation and the*  
1035 *atmosphere*, Monteith, J. L. (Ed.), Academic Press, New York, 57 –109, 1975.
- 1036 Tong, X., Li, J., Yu, Q., and Lin, Z.: Biophysical controls on light response of net CO<sub>2</sub> exchange in a winter  
1037 wheat field in the North China Plain, *PLoS ONE*, 9, e89469, doi:10.1371/journal.pone.0089469, 2014.
- 1038 U.S.G.S.: Mineral Commodity Summaries 2015 – Mercury, U. S. Geological Survey,  
1039 <http://minerals.usgs.gov/minerals/pubs/commodity/mercury/mcs-2015-mercu.pdf>, (last access:  
1040 September 2015), 2015.
- 1041 Wang, D. Y., He, L., Shi, X. J., Wei, S. Q., and Feng, X. B.: Release flux of mercury from different  
1042 environmental surfaces in Chongqing, China, *Chemosphere*, 64, 1845-1854, 2006.
- 1043 Wang, J., Wang, S., Jiang, J., Ding, A., Zheng, M., Zhao, B., Wong, D. C., Zhou, W., Zheng, G.,  
1044 Wang, L., Pleim, J. E., and Hao, J.: Impact of aerosol–meteorology interactions on fine particle  
1045 pollution during China’s severe haze episode in January 2013, *Environ. Res. Lett.*, 9, 094002, 2014a.

- 1046 Wang, L., Wang, S., Zhang, L., Wang, Y., Zhang, Y., Nielsen, C., McElroy, M. B., and Hao, J.: Source  
1047 apportionment of atmospheric mercury pollution in China using the GEOS-Chem model, *Environ.*  
1048 *Pollut.*, 190, 166-175, 2014b.
- 1049 Wang, L. T., Wei, Z., Yang, J., Zhang, Y., Zhang, F. F., Su, J., Meng, C. C., and Zhang, Q.: The 2013  
1050 severe haze over southern Hebei, China: model evaluation, source apportionment, and policy  
1051 implications, *Atmos. Chem. Phys.*, 14, 3151-3173, 2014c.
- 1052 Wang, S., Zhang, L., Wang, L., Wu, Q., Wang, F., and Hao, J.: A review of atmospheric mercury  
1053 emissions, pollution and control in China, *Front. Environ. Sci. Eng.*, 8, 631-649, 2014d.
- 1054 Wang, Z., Zhang, X., Xiao, J., Ci, Z., and Yu, P.: Mercury fluxes and pools in three subtropical  
1055 forested catchments, southwest China, *Environ. Pollut.*, 157, 801-808, 2009.
- 1056 Wen, L., Chen, J., Yang, L., Wang, X., Xu, C., Sui, X., Yao, L., Zhu, Y., Zhang, J., Zhu, T., and Wang,  
1057 W.: Enhanced formation of fine particulate nitrate at a rural site on the North China Plain in summer:  
1058 The important roles of ammonia and ozone, *Atmos. Environ.*, 101, 294-302, 2015.
- 1059 Wesely, M. L. and Hicks, B. B.: Some factors that affect the deposition rates of sulfur dioxide and  
1060 similar gases on vegetation., *J. Air Waste Manage.*, 27, 1110 - 1117, 1977.
- 1061 Wright, L. P. and Zhang, L. M.: An approach estimating bidirectional air-surface exchange for gaseous  
1062 elemental mercury at AMNet sites, *J. Adv. Model. Earth Syst.*, 7, 35-49, 2015.
- 1063 Xiao, Z. F., Munthe, J., Schroeder, W. H., and Lindqvist, O.: Vertical fluxes of volatile mercury over  
1064 forest soil and lake surfaces in Sweden, *Tellus B*, 43, 267-279, 1991.
- 1065 Xin, M. and Gustin, M. S.: Gaseous elemental mercury exchange with low mercury containing soils:  
1066 Investigation of controlling factors, *Appl. Geochem.*, 22, 1451-1466, 2007.
- 1067 Yang, Y. K., Zhang, C., Shi, X. J., Lin, T., and Wang, D. Y.: Effect of organic matter and pH on  
1068 mercury release from soils, *J. Environ. Sci.-China*, 19, 1349-1354, 2007.
- 1069 Zhang, H., Lindberg, S. E., and Kuiken, T.: Mysterious diel cycles of mercury emission from soils held  
1070 in the dark at constant temperature, *Atmos. Environ.*, 42, 5424-5433, 2008.
- 1071 Zhang, L., Blanchard, P., Gay, D. A., Prestbo, E. M., Risch, M. R., Johnson, D., Narayan, J., Zsolway,  
1072 R., Holsen, T. M., Miller, E. K., Castro, M. S., Graydon, J. A., St. Louis, V. L., and Dalziel, J.:  
1073 Estimation of speciated and total mercury dry deposition at monitoring locations in eastern and central  
1074 North America, *Atmos. Chem. Phys.*, 12, 4327-4340, 2012.
- 1075 Zhang, L., Wang, S. X., Wang, L., and Hao, J. M.: Atmospheric mercury concentration and chemical  
1076 speciation at a rural site in Beijing, China: Implications of mercury emission sources, *Atmos. Chem.*  
1077 *Phys.*, 13, 10505-10516, 2013.
- 1078 Zhang, Y. Q., Liu, R. H., Cui, Y. Q., Zhou, J. P., and Wang, Y.: The characteristic analysis of  
1079 atmospheric mercury during haze days in Qingdao, *China Env. Sci.*, 34, 1905-1911, 2014.
- 1080 Zhou, J., Feng, X., Liu, H., Zhang, H., Fu, X., Bao, Z., Wang, X., and Zhang, Y.: Examination of total  
1081 mercury inputs by precipitation and litterfall in a remote upland forest of Southwestern China, *Atmos.*  
1082 *Environ.*, 81, 364-372, 2013.
- 1083 Zhu, J. S., Wang, D. Y., Liu, X. A., and Zhang, Y. T.: Mercury fluxes from air/surface interfaces in  
1084 paddy field and dry land, *Appl. Geochem.*, 26, 249-255, 2011.
- 1085 Zhu, W., Sommar, J., Lin, C. -J., and Feng, X.: Mercury vapor air-surface exchange measured by  
1086 collocated micrometeorological and enclosure methods – Part I: Data comparability and method  
1087 characteristics, *Atmos. Chem. Phys.*, 15, 685-702, 2015a.
- 1088 Zhu, W., Sommar, J., Lin, C. -J., and Feng, X.: Mercury vapor air-surface exchange measured by  
1089 collocated micrometeorological and enclosure methods – Part II: Bias and Uncertainty Analysis,  
1090 *Atmos. Chem. Phys.*, 15, 5359-5376, 2015b.
- 1091 Zhu, Z., Sun, X., Zhao, F., and Meixner, F. X.: Ozone concentrations, flux and potential effect on yield  
1092 during wheat growth in the Northwest-Shandong Plain of China, *J. Environ. Sci. (China)*, 34, 1-9,  
1093 2015.